Original Article

Ferrostatin-1 attenuates hypoxic-ischemic brain damage in neonatal rats by inhibiting ferroptosis

Min Zhang[1,2,3,4], Zhiming Liu[5], Wei Zhou[1,2,3,4], Ming Shen[1,2,3,4], Niping Mao[1,2,3,4], Hang Xu[6], Yanan Wang[7], Zidi Xu[7], Mopu Li[7], Haibin Jiang[7], Yuetong Chen[6], Jianghu Zhu[1,2,3,4], Wei Lin[1,2,3,4], Junhui Yuan[8], Zhenlang Lin[1,2,3,4]

[1]Department of Pediatrics, the Second School of Medicine, the Second Affiliated Hospital and Yuying Children's Hospital of Wenzhou Medical University, Wenzhou, China; [2]Key Laboratory of Perinatal Medicine of Wenzhou, the Second Affiliated Hospital and Yuying Children's Hospital of Wenzhou Medical University, Wenzhou, China; [3]Key Laboratory of Structural Malformations in Children of Zhejiang Province, the Second Affiliated Hospital and Yuying Children's Hospital of Wenzhou Medical University, Wenzhou, China; [4]Zhejiang Provincial Clinical Research Center for Pediatric Disease, the Second Affiliated Hospital and Yuying Children's Hospital of Wenzhou Medical University, Wenzhou, China; [5]Department of Spinal Surgery, the Affiliated Hospital of Qingdao University, Qingdao, China; [6]The First School of Medicine, Wenzhou Medical University, Wenzhou, China; [7]The Second School of Medicine, Wenzhou Medical University, Wenzhou, China; [8]Department of Neonatology, Wenling Maternal and Child Health Care Hospital, Wenling, China

Contributions: (I) Conception and design: M Zhang, Z Liu; (II) Administrative support: W Lin, J Yuan, Z Lin; (III) Provision of study materials or patients: W Zhou, M Shen, N Mao, H Xu; (IV) Collection and assembly of data: Y Wang, Z Xu, M Li, H Jiang, Y Chen, J Zhu; (V) Data analysis and interpretation: M Zhang, Z Liu; (VI) Manuscript writing: All authors; (VII) Final approval of manuscript: All authors.

Correspondence to: Wei Lin, MD. Department of Pediatrics, the Second School of Medicine, the Second Affiliated Hospital and Yuying Children's Hospital of Wenzhou Medical University, No. 109 Xueyuan West Road, Wenzhou 325000, China; Key Laboratory of Perinatal Medicine of Wenzhou, the Second Affiliated Hospital and Yuying Children's Hospital of Wenzhou Medical University, No. 109 Xueyuan West Road, Wenzhou 325000, China; Key Laboratory of Structural Malformations in Children of Zhejiang Province, the Second Affiliated Hospital and Yuying Children's Hospital of Wenzhou Medical University, No. 109 Xueyuan West Road, Wenzhou 325000, China; Zhejiang Provincial Clinical Research Center for Pediatric Disease, the Second Affiliated Hospital and Yuying Children's Hospital of Wenzhou Medical University, No. 109 Xueyuan West Road, Wenzhou 325000, China. Email: linwei1110@163.com; Junhui Yuan, BM. Department of Neonatology, Wenling Maternal and Child Health Care Hospital, No. 102 Xiabao Road, Wenling 317500, China. Email: haiercha@126.com; Zhenlang Lin, MD. Department of Pediatrics, the Second School of Medicine, the Second Affiliated Hospital and Yuying Children's Hospital of Wenzhou Medical University, No. 109 Xueyuan West Road, Wenzhou 325000, China; Key Laboratory of Perinatal Medicine of Wenzhou, the Second Affiliated Hospital and Yuying Children's Hospital of Wenzhou Medical University, No. 109 Xueyuan West Road, Wenzhou 325000, China; Key Laboratory of Structural Malformations in Children of Zhejiang Province, the Second Affiliated Hospital and Yuying Children's Hospital of Wenzhou Medical University, No. 109 Xueyuan West Road, Wenzhou 325000, China; Zhejiang Provincial Clinical Research Center for Pediatric Disease, the Second Affiliated Hospital and Yuying Children's Hospital of Wenzhou Medical University, No. 109 Xueyuan West Road, Wenzhou 325000, China. Email: lzlprof2020@163.com.

Background: Hypoxic-ischemic brain damage (HIBD) is a type of brain damage that is caused by perinatal asphyxia and serious damages the central nervous system. At present, there is no effective drug for the treatment of this disease. Besides, the pathogenesis of HIBD remains elusive. While studies have shown that ferroptosis plays an important role in HIBD, its role and mechanism in HIBD are yet to be fully understood.

Methods: The HIBD model of neonatal rats was established using the Rice-Vannucci method. A complete medium of PC12 cells was adjusted to a low-sugar medium, and the oxygen-glucose deprivation model was established after continuous hypoxia for 12 h. Laser Doppler blood flow imaging was used to detect the blood flow intensity after modeling. 2,3,5-triphenyl tetrazolium chloride staining was employed to detect ischemic cerebral infarction in rat brain tissue, and hematoxylin and eosin staining and transmission electron microscopy were used to observe brain injury and mitochondrial damage. Immunofluorescence was applied to monitor the expression of GFAP. Real-time quantitative polymerase chain reaction, western blot, and immunofluorescence were utilized to detect the expression of messenger RNA and protein. The level of reactive oxygen species (ROS) in cells was detected using the ROS detection kit.

Results: The results showed that ferrostatin-1 (Fer-1) significantly alleviated the brain injury caused by hypoxia and ischemia. Fer-1 significantly increased the expression of SLC3A2, SLC7A11, ACSL3, GSS, and GPX4 ($P<0.05$) and dramatically decreased the expressions of GFAP, ACSL4, TFRC, FHC, FLC, 4-HNE, HIF-1α, and ROS ($P<0.05$).

Conclusions: Fer-1 inhibits ferroptosis and alleviates HIBD by potentially targeting the GPX4/ACSL3/ACSL4 axis; however, its specific mechanism warrants further exploration.

Keywords: Ferroptosis; hypoxic-ischemic brain damage (HIBD); oxygen-glucose deprivation (OGD); ferrostatin-1 (Fer-1)

Submitted Mar 22, 2023. Accepted for publication Nov 02, 2023. Published online Nov 20, 2023.
doi: 10.21037/tp-23-189
View this article at: https://dx.doi.org/10.21037/tp-23-189

Introduction

Hypoxic-ischemic brain damage (HIBD) in neonates is mainly caused by perinatal asphyxia, and its prevalence is about 1–6% (1). Nearly one-third of the survivors develop mental retardation, epilepsy, cerebral palsy, and other sequelae (2). Mild hypothermia is often used to treat HIBD; however, the clinical treatment of HIBD often misses its best therapeutic window and cannot significantly improve the prognosis of children with severe HIBD (3,4). Therefore, identifying new and effective treatment options for HIBD is crucial.

The pathogenesis of HIBD is yet to be completely understood. HIBD is mainly caused by inflammation, energy depletion, mitochondrial damage, calcium overload, and other factors (5-8). The relationship between ferroptosis and HIBD has been previously demonstrated. Zhu *et al.* found that inhibition of Toll-like receptor 4 (TLR4) reduced oxidative stress injury, the activation of ferroptosis, and the neuroinflammatory response induced by HIBD (9). Li *et al.* found that HIBD after modeling led to mitochondrial atrophy, brain atrophy/damage, and memory disorders (10). Our previous study found that lipid peroxidation, abnormal iron metabolism, and abnormal amino acid metabolism played important roles in HIBD (11). Vitamin D up-regulated the expression of nuclear factor erythroid 2-related factor 2 (Nrf2) and heme oxygenase 1 (HO-1) and inhibited the expression of glutathione peroxidase 4 (GPX4), superoxide dismutase (SOD), and glutathione (GSH), to reduce the ferroptosis of hypoxic-ischemic rats and further improve brain tissue injury (4). Our previous experiments found that HIBD increased the production of oxidative stress and inflammatory products, and then elevated reactive oxygen species (ROS) production to induce ferroptosis (12). Ginsenoside Rb1 (GsRb1) plays a neuroprotective role by reducing oxidative stress and inflammation and inhibiting ferroptosis, which indicates that GsRb1 might be used to treat hypoxic-ischemic encephalopathy, and also lays a foundation for the study of HIBD by inhibiting ferroptosis (12). While the above studies have indicated that ferroptosis is involved in the pathogenesis of HIBD, the specific molecular mechanisms of ferroptosis in HIBD warrant further exploration.

The concept of ferroptosis was first proposed by Dixon *et al.* in 2012 (13). Ferroptosis is a novel type of iron-dependent and ROS-reliant programmed cell death characterized by lipid peroxidation. It is precisely regulated

Highlight box

Key findings

- Both hypoxic-ischemic brain damage (HIBD) and Erastin caused changes in GPX4/ACSL3/ACSL4 expression to induce ferroptosis, while ferrostatin-1 (Fer-1) inhibited ferroptosis and reduced HIBD, indicating that the GPX4/ACSL3/ACSL4 axis is an important therapeutic target in HIBD.

What is known and what is new?

- Ferroptosis is involved in the pathogenesis of HIBD; however, the specific molecular mechanisms of ferroptosis in HIBD warrant further investigation.
- Fer-1 can inhibit ferroptosis and reduce HIBD, indicating that the GPX4/ACSL3/ACSL4 axis is an important therapeutic target in HIBD, and Fer-1 is a potential therapeutic target for HIBD.

What is the implication, and what should change now?

- Fer-1 inhibits HIBD-induced ferroptosis through the GPX4/ACSL3/ACSL4 axis, improves HIBD-induced ferroptosis in neurons, and reduces HIBD.

at multiple levels, including epigenetic, transcriptional, posttranscriptional, and posttranslational (14). In recent years, one study has shown that ferroptosis is closely related to the pathophysiological processes of various diseases, such as neurological diseases, ischemia and reperfusion injury, tumors, hematological diseases, and kidney injury, and how to intervene in the occurrence and development of related diseases by regulating ferroptosis has become a research hotspot (15).

Studies have shown that inhibiting the expression of microRNA-155 (MiR-155) can reduce inflammatory reaction and apoptosis by targeting sirtuin-1 (SIRT1) in HIBD (16). Atorvastatin activated the cAMP/PKA/p-CREB/BDNF pathway in the cerebral cortex after HIBD, inhibited the expression of Bax/Bcl2, improved the learning and memory ability, and reduced the apoptosis of neurons (17). In addition, hydrogen inhalation can inhibit the inflammatory reaction of microglia caused by HIBD, and reduce the expression of apoptotic factors, thus improving the long-term spatial memory deficit in the process of brain maturation caused by HIBD (18).

Heat shock protein B1 (HSPB1) is a negative regulator of ferroptosis. Overexpression of HSPB1 reduces ferritin levels in the hippocampus of HIBD rats, decreases apoptosis, and improves HIBD (19). Glycyrrhizin (GL) can improve oxidative stress imbalance and mitochondrial damage, thus reducing the production of inflammatory factors, ultimately reducing ferroptosis and cortical neuron damage after HIBD and inhibiting the occurrence and development of ferroptosis *in vivo* and *in vitro* (20).

One study found that Xenon (Xe) significantly reduced the expression of Beclin-1 and LC3-II induced by HIBD in rats, inhibited the formation of autophagy, significantly reduced the infarct volume of HIBD rats, and improved the nervous system defects (21). It has been found that the expression of colorectal neoplasia differentially expressed (CRNDE) in the brain increases in a time-dependent manner after HIBD, and silencing CRNDE can promote autophagy, thus reducing the pathological damage and apoptosis of the hippocampus in rats, reducing the infarct volume and improving the behavioral performance of HIBD rats (22). In addition, compared with the HIBD group, verbascoside (VB) reduced autophagy formation, Beclin-1 level, and LC3-II/I ratio of HIBD newborn rats and increased the level of P62, thus reducing the latency of neurological function and cerebral infarction volume and improving neuronal damage and degeneration (23).

Moreover, neferine significantly inhibited the messenger RNA (mRNA) expression of protein associated with pyroptosis in neonatal HIBD model rats, including caspase-1, the caspase adaptor apoptotic speck-like protein containing a caspase recruitment domain (ASC), Gasdermind, interleukin-18 (IL-18), IL-1β, and some inflammatory factors, thus improving neuroinflammation and oxidative stress injury (24). In addition, dexmedetomidine (Dex) inhibited the apoptosis of astrocytes induced by HIBD and the expression of inflammation-related factors by up-regulating miR-148a-3p, thus playing a protective role (25).

Herein, we hypothesize that ferrostatin-1 (Fer-1) inhibits ferroptosis and relieves HIBD in neonatal rats through the GPX4/acyl-CoA synthetase long-chain family member 3 (ACSL3)/acyl-CoA synthetase long-chain family member 4 (ACSL4) axis. We present this article in accordance with the ARRIVE reporting checklist (available at https://tp.amegroups.com/article/view/10.21037/tp-23-189/rc).

Methods

Experimental animal source

Specific pathogen-free (SPF) neonatal Sprague-Dawley (SD) rats (weight 200–300 g) were purchased from Zhejiang Weitong Lihua Test Animal Technology Co., Ltd. [SCXK (Zhejiang) 2019-0001]. All rats were kept in an SPF animal breeding room of the Animal Laboratory Center of Wenzhou Medical University, Wenzhou, China. The rats were allowed to freely mate at a ratio of 2:1 or 3:1 for females and males in each cage. After the female rats were pregnant, they were reared in separate cages. The neonatal rats that were born had free access to the female rats, which was recorded as P0 on the day of birth. The humidity and room temperature were maintained at about 60% and 22 ℃, respectively. A 12-hour day and night cycle was maintained with the lighting system. All the solid granulated feed and water were sterilized.

Grouping and processing of experimental animals

A total of 99 male SD rats (P7) were selected (males are the high-risk factors for HIBD in newborn rats) and randomly divided into the Sham operation group (Sham group), hypoxia-ischemia group (HIBD group), and hypoxia-ischemia + Fer-1 group (HIBD + Fer-1 group). To investigate the effect of Erastin, rats were randomly divided into the Sham group, HIBD group, and ferroptosis

inducer group (Erastin group) after modeling. To verify whether Fer-1 could reduce ferroptosis induced by Erastin, rats were randomly divided into the Sham group, Erastin group, and ferroptosis inducer + Fer-1 group (Erastin + Fer-1 group) after modeling. According to the needs of different experimental groups, different numbers of SD rats were selected to carry out corresponding experimental operations. All animal experiments were conducted under a project license (Ethics Batch No. wydw2022-0211) granted by the ethics committee of Wenzhou Medical University, in compliance with institutional guidelines for the care and use of animals.

Establishment of the HIBD model in neonatal rats

Male SD rats (P7) were selected and modeled according to the modified Rice-Vannucci method (26). First, rats were anesthetized with inhalation of isoflurane. After anesthesia, rats were fixed on the operating table. After the skin of the neck was disinfected with iodine, a 3–5 mm surgical incision was made in the middle of the neck. The left common carotid artery was bluntly separated and exposed with forceps using a microscope. The proximal and distal ends of the left common carotid artery were ligated with a suture [8-0]. The left common carotid artery was cut off between the two ligating wires. After disinfection with iodine, neonatal rats were daubed with female rat feces and allowed to rest in the female rat cage for 2 h. During this period, rats were free to ingest breast milk. After 2 h, the neonatal rats were placed in an anoxic box, where the temperature was maintained at about 37 ℃, nitrogen was continuously introduced into the anoxic box, the concentration of oxygen was maintained at about 8%, and the hypoxia lasted for 2.5 h. After hypoxia, neonatal rats were daubed with female rat feces again and put back in the original cage for continuous feeding. In the Sham group, only the left common carotid artery was exposed, and no ligation or hypoxia treatment was performed.

Animal dosing regimen

Fer-1 is a ferroptosis inhibitor (27). Approximately 5 mg of Fer-1 powder (Selleck, Houston, TX, USA) was dissolved in 2% dimethyl sulfoxide (DMSO) + 50% polyethylene glycol 300 (PEG 300) + 5% Tween 80 + double-distilled water (DDH_2O) to obtain a 5 mg/mL stock solution (ready-to-use). Rats in the HIBD + Fer-1 group received intraperitoneal injection of 10 mg/kg/d for 3 consecutive days (28-31).

Erastin is a ferroptosis inducer. About 5 mg of Erastin powder (Selleck) was dissolved in 5% dimethyl sulfoxide (DMSO) + 40% PEG 300 + 5% Tween 80 + DDH_2O, and 1.25 mg/mL of stock solution was obtained. Rats in the Erastin group received intraperitoneal injection of 10 mg/kg/d Erastin for 14 days (29,31).

Laser doppler blood flow imaging

Our previous study found that there was significant brain injury on the injury side at 72 h after HIBD modeling. Therefore, 72 h after HIBD modeling was also selected as the time point for subsequent studies (11).

On day 3 (P10), SD rats were positioned prone on the console and evaluated with a laser Doppler flow imager. Data were analyzed using Moor LDI Revision (ver.6.1; Moor Instruments, Axminster, UK) and perfusion units (PU) to assess flow intensity.

Brain tissue water content detection

After the third postoperative day (P10), brain tissue was removed from the left side (mold side) and weighed (wet weight). The weighted brain tissue was then placed in an oven (100 ℃) for 72 h and weighed (dry weight). Brain water content was calculated using the following formula: dry-wet weight ratio = (wet weight – dry weight)/wet weight × 100%.

2,3,5-triphenyl tetrazolium chloride (TTC) staining

TTC staining is often used to detect ischemic infarction in rat brain tissue. After 72 h of molding, rats were anesthetized with isoflurane, fixed on the operating table in the supine position, and fully exposed to the heart. The perfusion needle was stabbed into the left ventricle, the right ear was cut open, and brain tissue was harvested after perfusion with 40 mL of pre-cooled phosphate-buffered saline (PBS). Brain tissue was frozen at –80 ℃ for about 5 min, and then cut into 5–6 coronal slices every 2 mm apart. The brain slices were then tiled in 1% TTC solution (Sigma-Aldrich, St. Louis, MO, USA) and incubated at 37 ℃ for 30 min on a shaker in the dark. Image J software

was used to analyze the volume of infarcted area in brain slices. Percentage of infarct volume of brain tissue = (sum of ischemic volumes of each slice)/(sum of volumes of each slice) × 100%.

Hematoxylin and eosin (H&E) staining

After 72 h of HIBD modeling, rats were infused with 20 mL of PBS and 20 mL of 4% paraformaldehyde (PFA), as previously described (12). After perfusion, brain tissues were incubated with 4% PFA at 4 ℃ overnight in a refrigerator. The fixed brain tissues were taken out on the next day and the front and rear thirds were cut off. Subsequently, ethanol dehydration and xylene transparentizing were performed, followed by paraffin embedding. The embedded paraffin blocks were cut into 5 μm thick coronal sections and fixed on slides. The slides were dried, waxed in an oven at 65 ℃ for 1 h, deparaffinized by xylene I and II, hydrated by gradient ethanol, subjected to hematoxylin staining, tap water rinsing, returned to differentiation solution blue, eosin staining, ethanol dehydration, xylene transparentizing, and neutral gum sealing, and then placed under an optical microscope (Favor Cai Optical Instrument Co., Ltd., Shanghai, China) for observation and imaging after ventilation.

Transmission electron microscopy (TEM) detection

After 3 days of modeling, the brain tissue was taken, and the hippocampus was isolated and cut into 1 mm^3 tissue slices for TEM detection. The tissues or cells were then placed in a pre-cooled electron microscope fixative and fixed at 4 ℃ for 2 h. After 1% osmic acid fixation, room temperature gradient ethanol dehydration, infiltration embedding, etc., tissues or cells were cut into 60–80 nm ultra-thin sections, stained with uranium-lead double staining, dried at room temperature, observed under a TEM (Hitachi, HT7800, Tokyo, Japan), a then images were collected for analysis. To ensure that the samples used for TEM were sampled in the same way in different groups, the same experimenter used the same protocol to conduct experiments on the same batch of rats or cells and used the same scale with the same multiple to collect the target tissues or cells in the target area.

Immunofluorescence

For *in vivo* experiments, brain tissue was taken after 72 h of modeling with HIBD and injected with PBS and 4% PFA. After paraffin embedding, slices were baked, conventionally dewaxed with water, repaired with citrate repair solution (C1010, Solarbio, Beijing, China) via heating at high temperature, cooled for 2 h, and washed. For *in vitro* experiments, cells were collected after 12 h of modeling with oxygen-glucose deprivation (OGD), fixed with 4% PFA for 1 h after washing, and permeabilized with 0.5% Triton X-100 at room temperature for 20 min.

Brain tissue sections or cells were blocked with 10% goat serum at room temperature for 30 min and then incubated with glial fibrillary acidic protein (GFAP; 1:200, #3670, Cell Signaling Technology, Danvers, MA, USA) and ACSL3 (1:200, A22085, ABclonal, Wuhan, China) at 4 ℃ overnight in a refrigerator. Subsequently, samples were rewarmed at 37 ℃ for 30 min on a shaker and then incubated with suitable fluorescent secondary antibodies (1:250, SA00013-1, Proteintech, Wuhan, China) (1:250, SA00013-2, Proteintech) at room temperature for 2 h after washing. Brain tablets were washed, sealed with a 4',6-diamidino-2-phenylindole (DAPI)-containing anti-fluorescence attenuation sealing tablet (S2110, Solarbio), and finally observed and photographed with a fluorescence microscope (Ningbo Yongxin Optical Co., Ltd., Ningbo, China).

Western blot assay

For animal experiments, brain tissues were taken after 3 days of HIBD modeling. For cell experiments, cells were collected at the end of 12 h of cell OGD modeling/Erastin treatment and adequately washed with PBS. The tissues or cells were lysed with a mixture of radioimmunoprecipitation assay (RIPA) lysate (P0013B, Beyotime, Shanghai, China) and protease inhibitor (P1046, Beyotime) (tissues were fully homogenized with a homogenizer and cells were crushed using an ultrasonic machine). Cells were lysed on ice for 30 min and centrifuged at 12,000 g for 20 min before cooling at 4 ℃ to obtain the supernatant. The protein concentration of the tissues/cells to be tested was then detected using the BCA protein quantitation/concentration assay kit (Cat:MA0082, Meilunbio, Dalian, China), and the loading protein was finally prepared according to the 20 μL system. The target proteins with different molecular weights were separated using 6–12.5% sodium dodecyl sulfate-polyacrylamide gel electrophoresis (SDS-PAGE). Proteins were transferred to a membrane, which was then blocked using 5% skim milk at room temperature for 2 h. Membranes were incubated with primary antibodies at 4 ℃

Table 1 Primers used in the polymerase chain reaction

Gene name	Primer	Sequence (5'-3')
SLC3A2	Forward	AGTGTGTCGCAGGCAGGA
	Reverse	TGGCAGAGTGAAGAGCAG
SLC7A11	Forward	ACGGTGGTGTGTTTGCTG
	Reverse	GGAGTGTGCTTGTGGACG
ACSL3	Forward	TGGAGAGTTTGACCCTGA
	Reverse	CCGTTAAATCCTTTCGTT
ACSL4	Forward	GCTCCTCTTATTTGCTGT
	Reverse	CCTTTGTCCATTTTCATC
TFRC	Forward	AGAACAAAAAGAGGAGTG
	Reverse	GCGAGAAGATTTAGGAAC
FHC	Forward	AACTTCACAAACTGGCTA
	Reverse	TCTTTAATGGATTTCACC
FLC	Forward	CTCTGGGCTTCTTTTTTG
	Reverse	TCTTGAGATGGCTTCTGC
GSS	Forward	GAGCCTCCTACATCCTCA
	Reverse	ACTCCAAAAATACCCAGC
GPX4	Forward	GCCGAGTGTGGTTTACGA
	Reverse	CTTGGGCTGGACTTTCAT
HIF-1α	Forward	TCGGACAACCTCACCAGA
	Reverse	GAAAAAGGGAGCCATCAT
GAPDH	Forward	GGCTCTCTGCTCCTCCCTGT
	Reverse	CGTTCACACCGACCTTCACC

SLC3A2, solute carrier family 3 member 2; SLC7A11, solute carrier family 7 member 11; ACSL3, acyl-CoA synthetase long-chain family member 3; ACSL4, acyl-CoA synthetase long-chain family member 4; TFRC, transferrin receptor; FHC, ferritin heavy chain; FLC, ferritin light chain; GSS, glutathione synthetase; GPX4, glutathione peroxidase 4; HIF-1α, hypoxia-inducible factor-1α; GAPDH, glyceraldehyde-3-phosphate dehydrogenase.

overnight after washing. The following primary antibodies were used in the above experiments: solute carrier family 3, member 2 (SLC3A2; 1:1,000, A5702, ABclonal), solute carrier family 7, member 11 (SLC7A11; 1:1,000, A2413, ABclonal), ACSL3 (1:1,000, A22085, ABclonal), ACSL4 (1:1,000, A20414, ABclonal), transferrin receptor (TFRC; 1:1,000, A18083, ABclonal), ferritin heavy chain (FHC; 1:1,000, A19544, ABclonal), ferritin light chain (FLC; 1:1,000, A18051, ABclonal), glutathione synthetase (GSS; 1:1,000, A14535, ABclonal), GPX4 (1:2,000, A1933, ABclonal), 4-hydroxynonenal (4-HNE; 1:2,000, Ab46545, Abcam, Cambridge, UK), hypoxia-inducible factor-1α (HIF-1α; 1:2,000, 20960-1-AP, Proteintech), and beta-actin (β-actin; 1:10,000, T0022, Affinity, Nottingham, UK). Subsequently, the membrane was washed and incubated with the corresponding secondary antibody (goat anti-mouse, 1:500, SE132, Solarbio; goat anti-rabbit, 1:5,000, SE134, Solarbio) at room temperature 2 h. Next, the bands were exposed to a Bio-Rad imaging system. The gray values of each band were then analyzed using Image Lab 6.1 software (Bio-Rad, Hercules, CA, USA) and Image J 1.50 software (National Institutes of Health, Bethesda, MD, USA). Each experiment was performed at least three times.

Real-time quantitative polymerase chain reaction (RT-qPCR)

Total RNA from brain tissues and cells was extracted using a centrifuge column RNAeasy^{TM} RNA extraction kit (R0026, Beyotime), and RNA concentration was determined using an optical density (OD)260/OD280 ratio determined by an ultraviolet spectrophotometer (Thermo Fisher Scientific, Waltham, MA, USA). The extracted RNA was reverse-transcribed into complementary DNA (cDNA). RT-qPCR was run on a CFX96TM real-time PCR detection system (Bio-Rad). The thermal cycle conditions were: 95 ℃ initial denaturation for 30 s followed by 40 cycles of 95 ℃ for 10 s; 60 ℃ for 30 s; 95 ℃ for 15 s. The required primer sequences were designed in GenBank and are summarized in *Table 1*. The expression of target genes was calculated using the $2^{-\Delta\Delta CT}$ method, with β-actin mRNA level as the internal reference.

Cell culture and grouping

PC12 cells (differentiated) were purchased from the Cell Bank of China Academy of Sciences (Shanghai, China). 10% fetal bovine serum (FBS; Gibco, Grand Island, NY, USA, Cat:10100147) was added to Dulbecco's modified Eagle medium (DMEM; Gibco, Cat:11965092) and incubated at 37 ℃ in a humidified incubator with 5% CO_2 atmosphere.

After achieving an 80% confluence, cells were randomly divided into the Control group, OGD group, and OGD + Fer-1 group. To study the effect of Erastin, cells were randomly divided into the Control group, OGD group, and Erastin group. To verify whether Fer-1 could reduce

Erastin-induced ferroptosis, cells were randomly divided into the Control group, Erastin group, and Erastin + Fer-1 group.

Cell administration protocol and establishment of an OGD model

To determine the optimal concentration of Fer-1 for inhibiting OGD-induced ferroptosis in PC12 cells, cells were treated with Fer-1 at different concentration gradients (0, 0.5, 1, 1.5, and 2 μM) after modeling with OGD, and cell viability was measured using the Cell Counting Kit-8 (CCK-8; Cat:MA0218, Meilunbio). The results suggested that treatment with 1 μM Fer-1 significantly improved the cell viability after OGD modeling; thus, 1 μM Fer-1 was selected for subsequent analysis.

To determine the optimal concentration of Erastin for the induction of ferroptosis by PC12 cells, cells were treated with different concentration gradients (0, 2.5, 5, 7.5, and 10 μM) at the early stage, and detected the cell activity using a CCK-8 assay. Finally, the concentration of Erastin used in cell intervention was determined to be 7.5 μM.

The complete medium of PC12 cells was replaced with low-glucose DMEM (Gibco, Cat:11054001) and an FBS-free medium. Then, according to the experimental requirements, OGD and OGD + Fer-1 groups were placed in a hypoxia incubator for hypoxia (5% CO_2, 95% N_2), respectively (32), which continued for 12 h. For Erastin and Erastin + Fer-1 groups, Erastin (7.5 μM) and/or Fer-1 (1 μM) were added for continuous action for 12 h. After hypoxia at 37 ℃ and drug treatment for 12 h, cells of each group were re-added with the basic medium and cultured in an incubator for 2 h. Cells in the Control group were not subjected to hypoxia treatment or replaced with FBS-free and low-glucose medium. Cells in all the different groups were collected after 2 h for subsequent analysis.

Cell reactive oxygen measurement

The ROS assay kit (Cat:CA1410, Solar Biology) was used to detect intracellular levels of ROS. According to the reagent instructions, 2',7'-dichlorodihydrofluorescein diacetate (DCFH-DA) was diluted and added to different groups for incubation in a cell incubator for about 30 min. After the cells were fully washed, they were collected (at least 1×10^5 cells per tube), re-suspended, and detected using the up-flow cytometry (Beckman Coulter, Brea, CA, USA) and analyzed using FlowJo 10.6.2 software.

Statistical analysis

All experimental data were analyzed using SPSS 23.0 Statistical Software (IBM Corp., Armonk, NY, USA). Quantitative data were expressed as the mean ± standard deviation of at least three independent experiments. One-way analysis of variance (ANOVA) was utilized for comparison of more than two groups, and the least significant difference (LSD) was used for comparison between the two groups. $P<0.05$ was considered statistically significant.

Results

HIBD modeling results

To explore whether the HIBD model was successfully established, we measured the blood flow on the brain surface using a laser Doppler 72 h after modeling. It was found that the blood flow signal intensity on the left side of the HIBD group was significantly lower relative to that on the left side of the Sham group. Notably, there was no significant difference in blood flow signal intensity on both sides of the Sham group. However, the blood flow signal intensity on the left side of HIBD group was significantly lower compared with that on the right side (*Figure 1A-1D*). These results indicated that the HIBD model was successfully established. Comparison of the water content of brain tissues in different groups and examination of the morphology revealed that compared with the Sham group, the brain tissues in the HIBD group were liquefied, necrotic and atrophic, and the brain water content was decreased. Treatment with Fer-1 significantly improved the atrophy and damage of brain tissue after hypoxia-ischemia and the water content of brain tissue was significantly increased (*Figure 1E,1F*). Subsequently, we performed TTC staining and quantitative analysis of the infarct volume percentage of brain tissue 72 h after modeling HIBD. There was significant cerebral infarction in brain tissue, and Fer-1 treatment effectively improved the cerebral infarction (*Figure 1G,1H*). The HE staining diagram of the brain tissue on day 3 after modeling is presented in *Figure 1I,1J*. After hypoxic-ischemic injury, the hippocampus on the modeling side of HIBD significantly shrank and reduced in size, and the cerebral cortex and hippocampus (CA1, CA3, and DG regions) exhibited disordered structure and cell

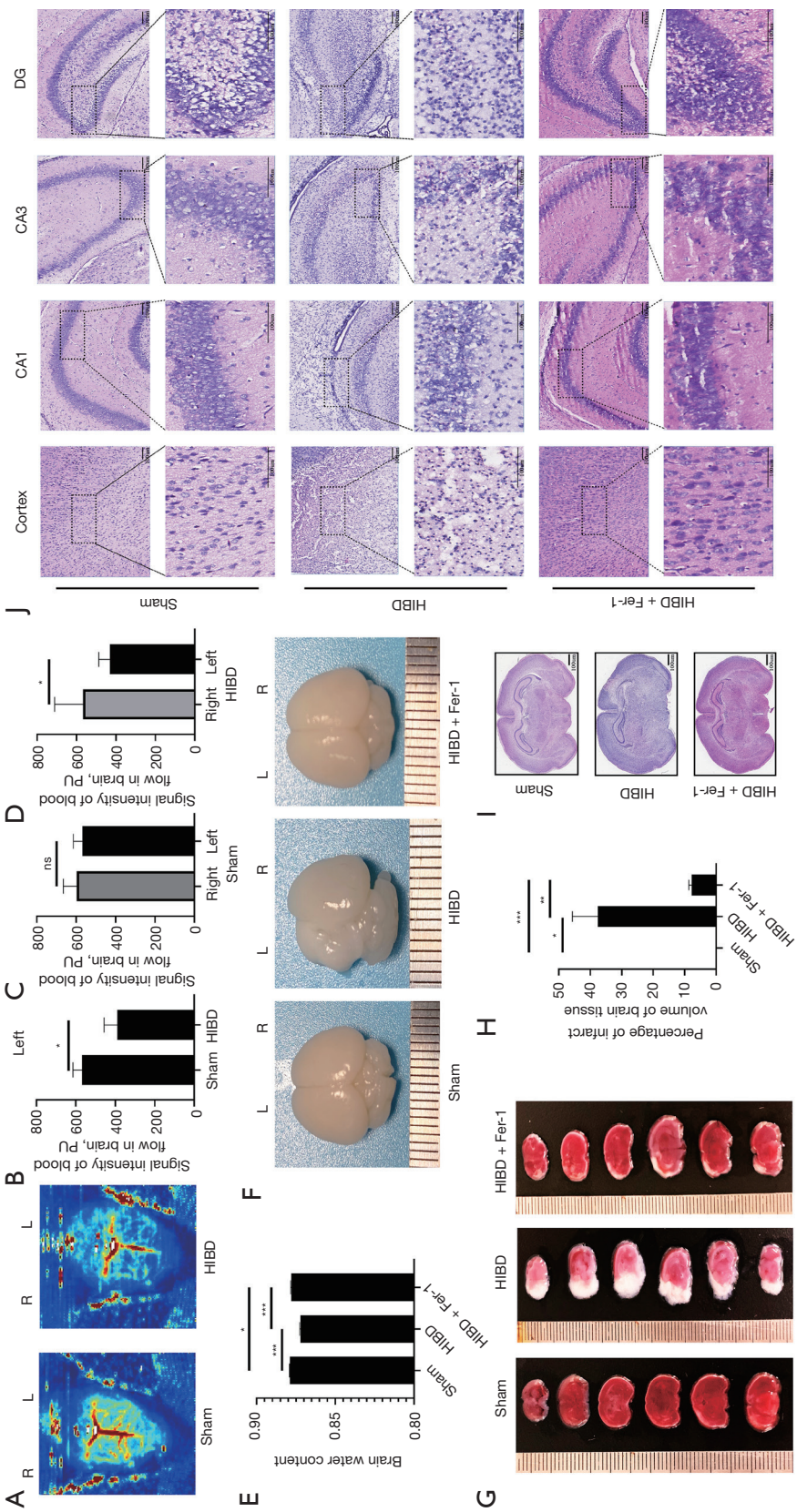

Figure 1 Hypoxic ischemia causes significant brain damage. (A) Blood flow on the surface of cerebral cortex in the indicated groups. (B) A histogram showing the intensity of blood flow signals in the two groups. (C) A histogram displaying the blood flow signal intensity on the left and right sides of the Sham group. (D) The histogram showing the blood flow signal intensity on the left and right sides of the HIBD group. (E) The histogram displaying the dry-wet weight ratio in different groups. (F) Brain tissues were isolated from 72 h after modeling with HIBD. (G) Representative results of TTC staining in coronary brain sections 72 h after HIBD modeling. (H) The histogram indicating the percentage of infarct volume of brain tissue in different groups. (I) Representative images of H&E staining at 3 d after HIBD molding. (J) Representative images of H&E staining of the cortex and hippocampus CA1, CA3, and DG of the damaged side of the brain at 72 h after HIBD modeling. Scale bar 100 μm. Mean ± standard deviation, n=3. *, P<0.05; **, P<0.01; ***, P<0.001, indicate significant differences; ns represents no significant difference. R, right; L, left; HIBD, hypoxic-ischemic brain damage; PU, perfusion units; Fer-1, ferrostatin-1; CA, cornu ammonis; DG, dentate gyrus; TTC, 2,3,5-triphenyl tetrazolium chloride; H&E, hematoxylin and eosin.

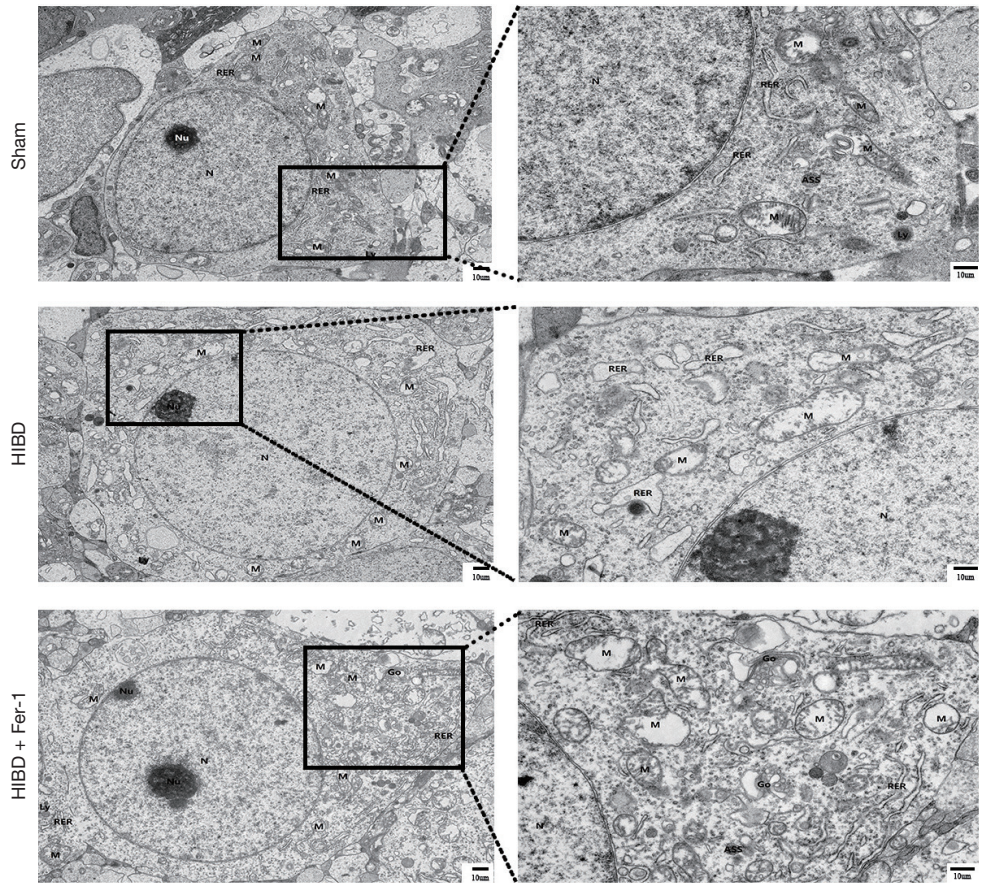

Figure 2 Seventy-two hours after modeling with HIBD (P10), representative TEM images showing the hippocampus on the modeled side from different groups. Different cellular structures are labeled. Scale bar 10 μm. M, mitochondria; RER, rough endoplasmic reticulum; Nu, nucleolus; N, nucleus; ASS, autolysosome; Ly, lysosome; HIBD, hypoxic-ischemic brain damage; Fer-1, ferrostatin-1; Go, golgi apparatus; TEM, transmission electron microscopy.

arrangement, accompanied by karyopycnosis, degeneration, and necrosis, among other disruption features. Fer-1 treatment significantly accelerated the morphological repair after HIBD modeling. The bilateral hippocampus exhibited symmetry, with well-organized cells in both the cerebral cortex and hippocampus displaying distinct chromatography.

Upon examination with TEM, it was observed that compared with the Sham group, significant alterations were observed in the mitochondrial structure post-HIBD modeling. This included extensive dissolution of the mitochondrial matrix, disappearance of cristae, and the emergence of vacuoles. Notably, the administration of Fer-1 substantially ameliorated these changes, leading to an improved mitochondrial morphology and structure, as depicted in *Figure 2*.

Several markers of brain injury have been reported. GFAP is mainly expressed in the nervous system and is a marker of astrocytes (33). Astrocyte proliferation causes up-regulation of GFAP following damage to the central nervous system (34). Measuring the expression of GFAP can help to explore whether the establishment of the HIBD model is successful (11). Compared with the Sham group, the expression of GFAP in the lateral cortex and hippocampus of rats in the HIBD group was significantly increased. Interestingly, Fer-1 treatment significantly reduced the proliferation of astrocytes after hypoxia-ischemia and down-regulated GFAP expression

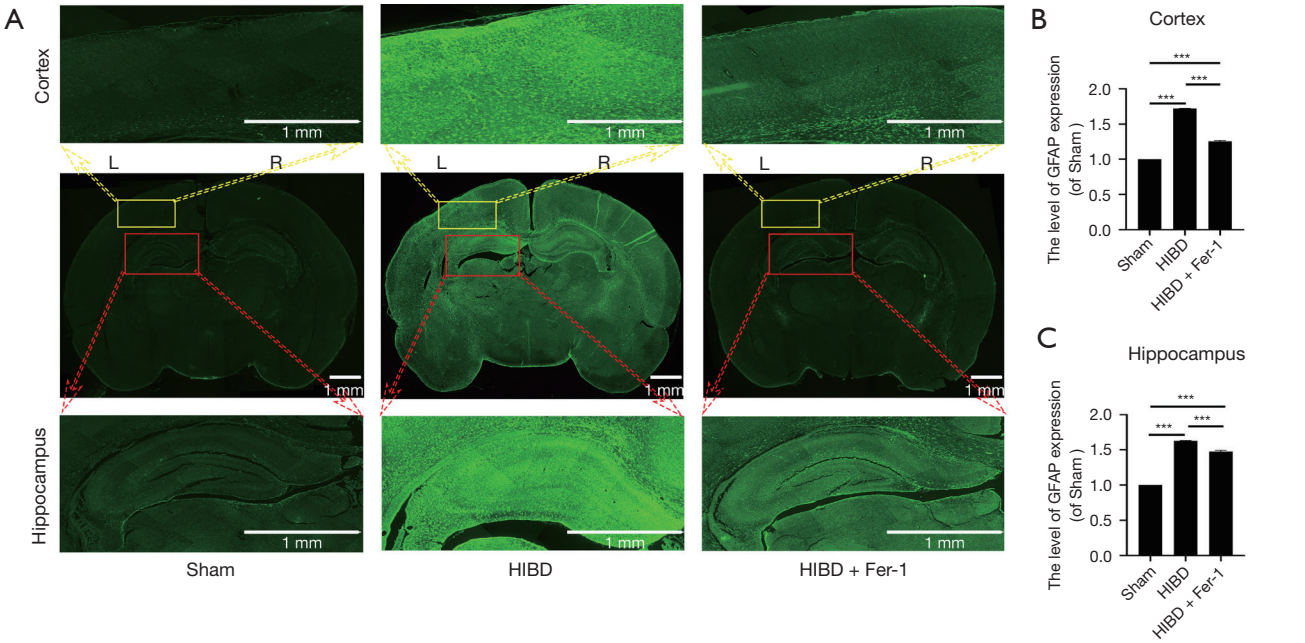

Figure 3 Proliferation and activation of astrocytes after modeling with HIBD. (A) Representative images of immunohistochemical staining of GFAP in various groups at 72 h after HIBD. (B,C) The histogram showing the average integrated density of GFAP positive staining in different groups of cortex and hippocampus. Mean ± standard deviation, n=3. ***, P<0.001, indicate significant differences. L, left; R, right; HIBD, hypoxic-ischemic brain damage; Fer-1, ferrostatin-1; GFAP, glial fibrillary acidic protein.

(*Figure 3A-3C*).

Fer-1 improved the activities of System Xc and ACSL3/ ACSL4 and alleviated HIBD

System Xc is an amino acid reverse transporter, consisting of SLC3A2 and SLC7A11, which facilitates the transmembrane exchange of intracellular glutamate and extracellular cystine (35,36). In this experiment, after HIBD/OGD modeling and Erastin treatment, the protein and mRNA expression levels of SLC3A2 and SLC7A11 decreased significantly, and treatment with Fer-1 significantly reversed this trend (*Figures 4-11*). Collectively, these results indicated that Fer-1 effectively improved the activity of System Xc.

The acyl-CoA synthetase long-chain family (ACSLs) consists of five members, ACSL1, 3, 4, 5, and 6 (37). ACSL3 regulates susceptibility to ferroptosis through a mechanism dependent on exogenous fatty acid composition (38). Some scholars have found that activation of monounsaturated fatty acids (MUFAs) by ACSL3 can reduce the sensitivity of plasma membrane lipids to oxidation thereby reducing the effects of ferroptosis on cells (39). Compared with the Sham group, HIBD/OGD modeling and Erastin caused a significant decrease in ACSL3 protein and mRNA expressions, while Fer-1 treatment significantly improved this phenomenon (*Figures 4-11*). This phenomenon was also confirmed by the results of cellular immunofluorescence analysis of ACSL3 (*Figure 12A,12B*), suggesting that Fer-1 increased the activity of ACSL3 and inhibited the ferroptosis.

Studies have found that specific knock-out of ACSL4 inhibits Erastin-induced cell ferroptosis. Overexpression of ACSL4 restores the sensitivity of cells to Erastin. Thus, ACSL4 is not only a sensitive marker of ferroptosis but also an important factor contributing to ferroptosis development (40). The experimental results demonstrated that HIBD and Erastin upregulated the expression level of ACSL4 protein and mRNA, and Fer-1 inhibited the expression of ACSL4 (*Figures 4-11*).

Changes in expression of iron metabolism-related proteins

Iron metabolism plays an important role in the regulation of Fenton reaction and production of ROS. It is also an indispensable factor in the initiation of ferroptosis (41,42).

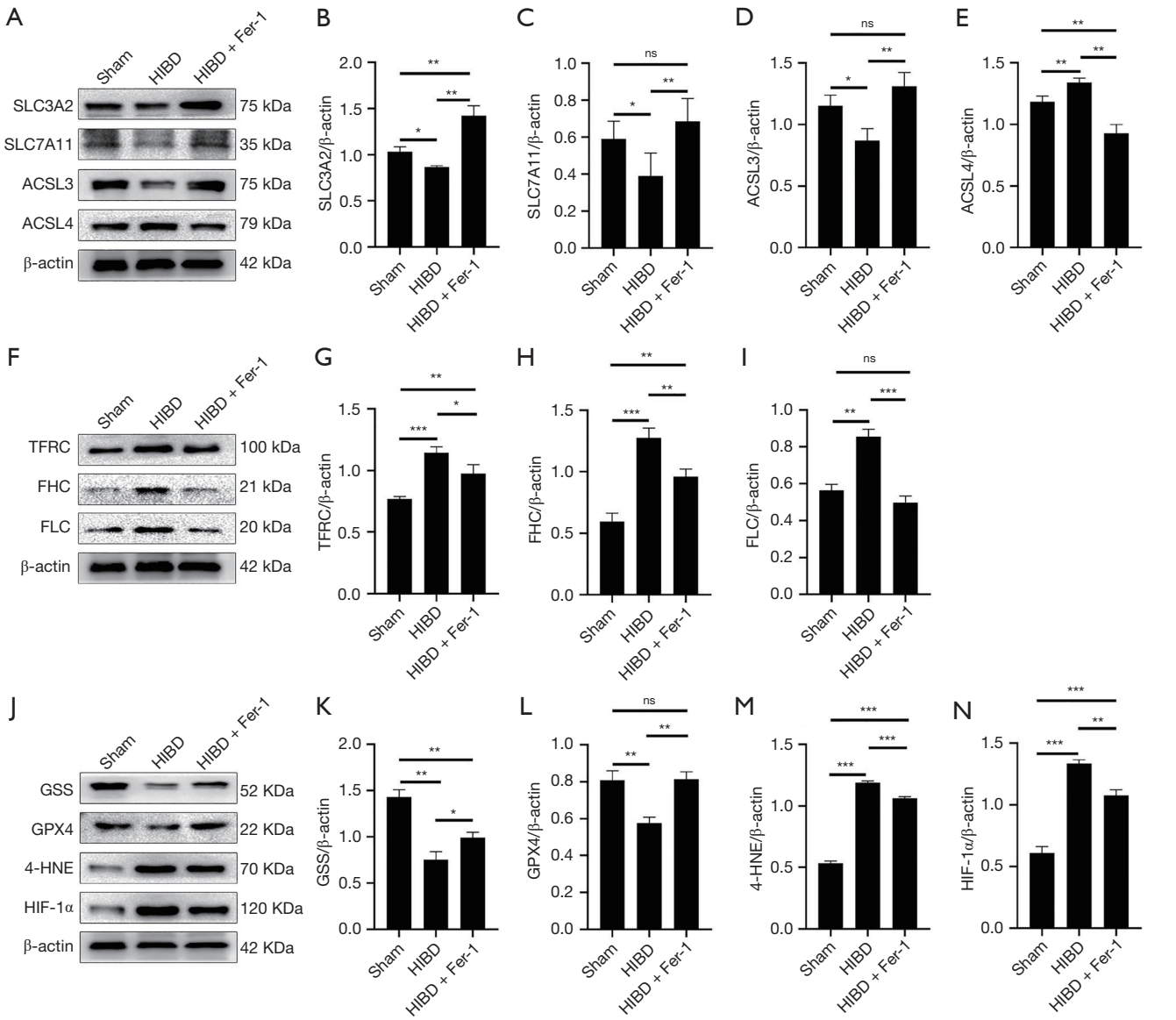

Figure 4 Fer-1 attenuates HIBD-induced ferroptosis. (A-N) Representative western blot images and quantitation of SLC3A2, SLC7A11, ACSL3, ACSL4, TFRC, FHC, FLC, GSS, GPX4, 4-HNE, and HIF-1α at 72 h after HIBD modeling (normalized to β-actin). Mean ± standard deviation, n=3. *, P<0.05; **, P<0.01; ***, P<0.001, indicate significant differences; ns represents no significant difference. HIBD, hypoxic-ischemic brain damage; Fer-1, ferrostatin-1; SLC3A2, solute carrier family 3, member 2; SLC7A11, solute carrier family 7, member 11; ACSL3, acyl-CoA synthetase long-chain family member 3; ACSL4, acyl-CoA synthetase long-chain family member 4; TFRC, transferrin receptor; FHC, ferritin heavy chain; FLC, ferritin light chain; GSS, glutathione synthetase; GPX4, glutathione peroxidase 4; 4-HNE, 4-hydroxynonenal; HIF-1α, hypoxia-inducible factor-1α.

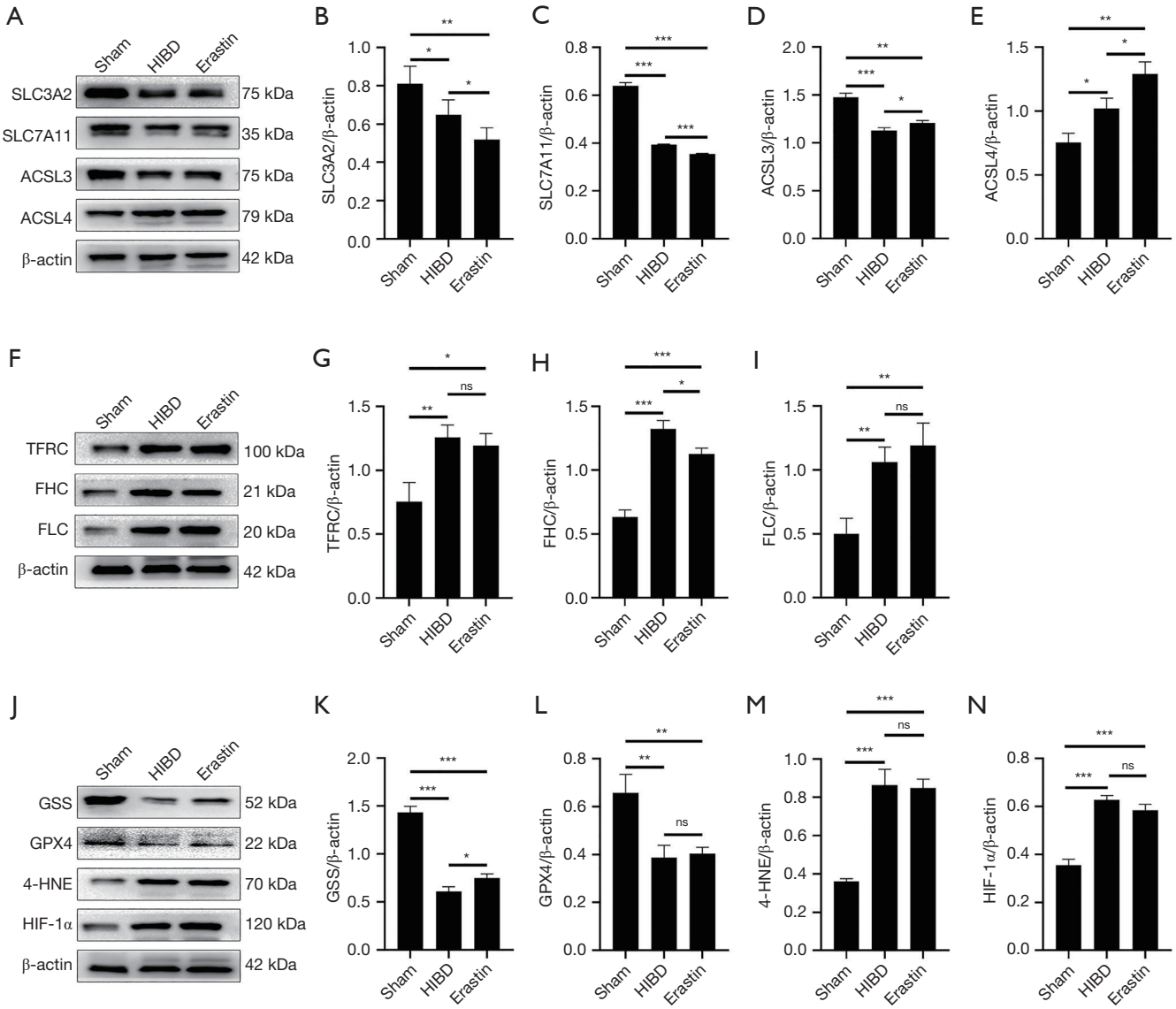

Figure 5 Both HIBD modeling and Erastin could induce ferroptosis. (A-N) Representative western blot images and quantitation of SLC3A2, SLC7A11, ACSL3, ACSL4, TFRC, FHC, FLC, GSS, GPX4, 4-HNE, and HIF-1α after HIBD modeling and injection of Erastin (normalized to β-actin). Mean ± standard deviation, n=3. *, P<0.05; **, P<0.01; ***, P<0.001, indicate significant differences; ns represents no significant difference. HIBD, hypoxic-ischemic brain damage; SLC3A2, solute carrier family 3, member 2; SLC7A11, solute carrier family 7, member 11; ACSL3, acyl-CoA synthetase long-chain family member 3; ACSL4, acyl-CoA synthetase long-chain family member 4; TFRC, transferrin receptor; FHC, ferritin heavy chain; FLC, ferritin light chain; GSS, glutathione synthetase; GPX4, glutathione peroxidase 4; 4-HNE, 4-hydroxynonenal; HIF-1α, hypoxia-inducible factor-1α.

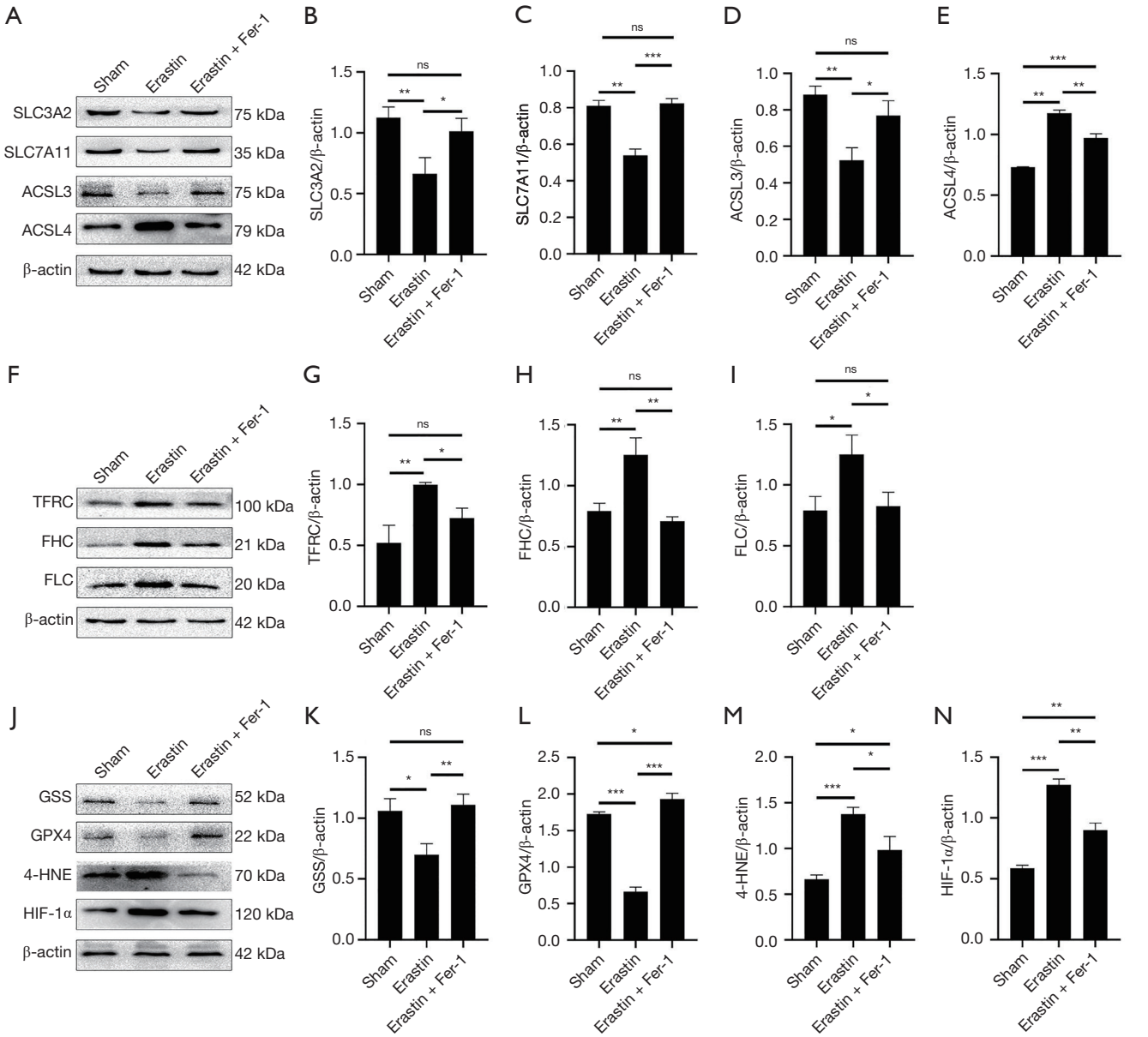

Figure 6 Fer-1 can inhibit ferroptosis induced by Erastin. (A-N) Representative western blot images and quantitation of SLC3A2, SLC7A11, ACSL3, ACSL4, TFRC, FHC, FLC, GSS, GPX4, 4-HNE, and HIF-1α 14 d after the injection of Erastin (normalized to β-actin). Mean ± standard deviation, n=3. *, P<0.05; **, P<0.01; ***, P<0.001, indicate significant differences; ns represents no significant difference. HIBD, hypoxic-ischemic brain damage; Fer-1, ferrostatin-1; SLC3A2, solute carrier family 3, member 2; SLC7A11, solute carrier family 7, member 11; ACSL3, acyl-CoA synthetase long-chain family member 3; ACSL4, acyl-CoA synthetase long-chain family member 4; TFRC, transferrin receptor; FHC, ferritin heavy chain; FLC, ferritin light chain; GSS, glutathione synthetase; GPX4, glutathione peroxidase 4; 4-HNE, 4-hydroxynonenal; HIF-1α, hypoxia-inducible factor-1α.

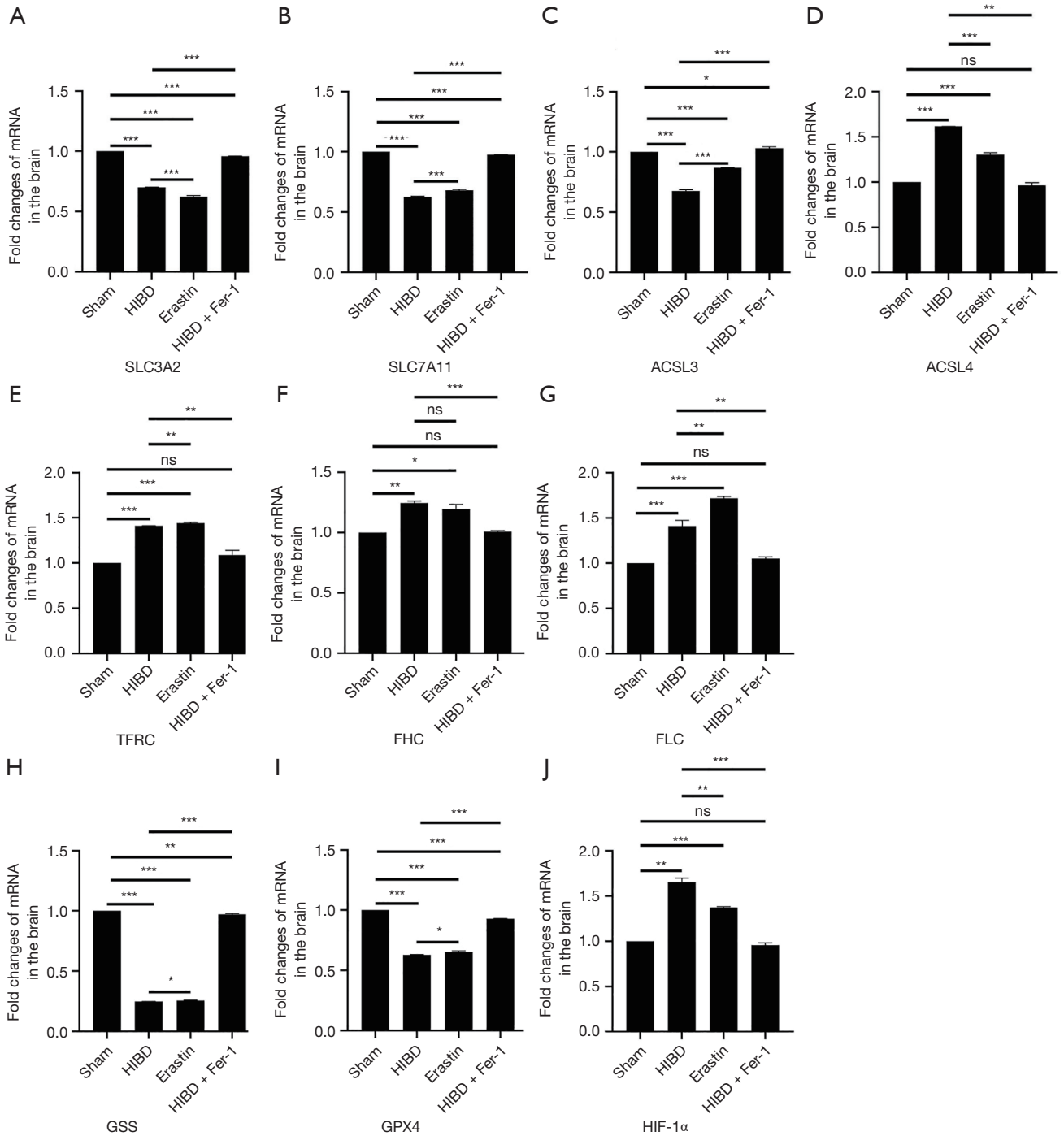

Figure 7 Change of mRNA expression levels of the ferroptosis-related gene in different groups *in vivo*. (A-J) The levels of SLC3A2, SLC7A11, ACSL3, ACSL4, TFRC, FHC, FLC, GSS, GPX4, and HIF-1α of mRNA expression in the brain tissue normalized to those of β-actin for each sample. Mean ± standard deviation, n=3. *, P<0.05; **, P<0.01; ***, P<0.001, indicate significant differences; ns represents no significant difference. mRNA, messenger RNA; HIBD, hypoxic-ischemic brain damage; Fer-1, ferrostatin-1; SLC3A2, solute carrier family 3, member 2; SLC7A11, solute carrier family 7, member 11; ACSL3, acyl-CoA synthetase long-chain family member 3; ACSL4, acyl-CoA synthetase long-chain family member 4; TFRC, transferrin receptor; FHC, ferritin heavy chain; FLC, ferritin light chain; GSS, glutathione synthetase; GPX4, glutathione peroxidase 4; HIF-1α, hypoxia-inducible factor-1α.

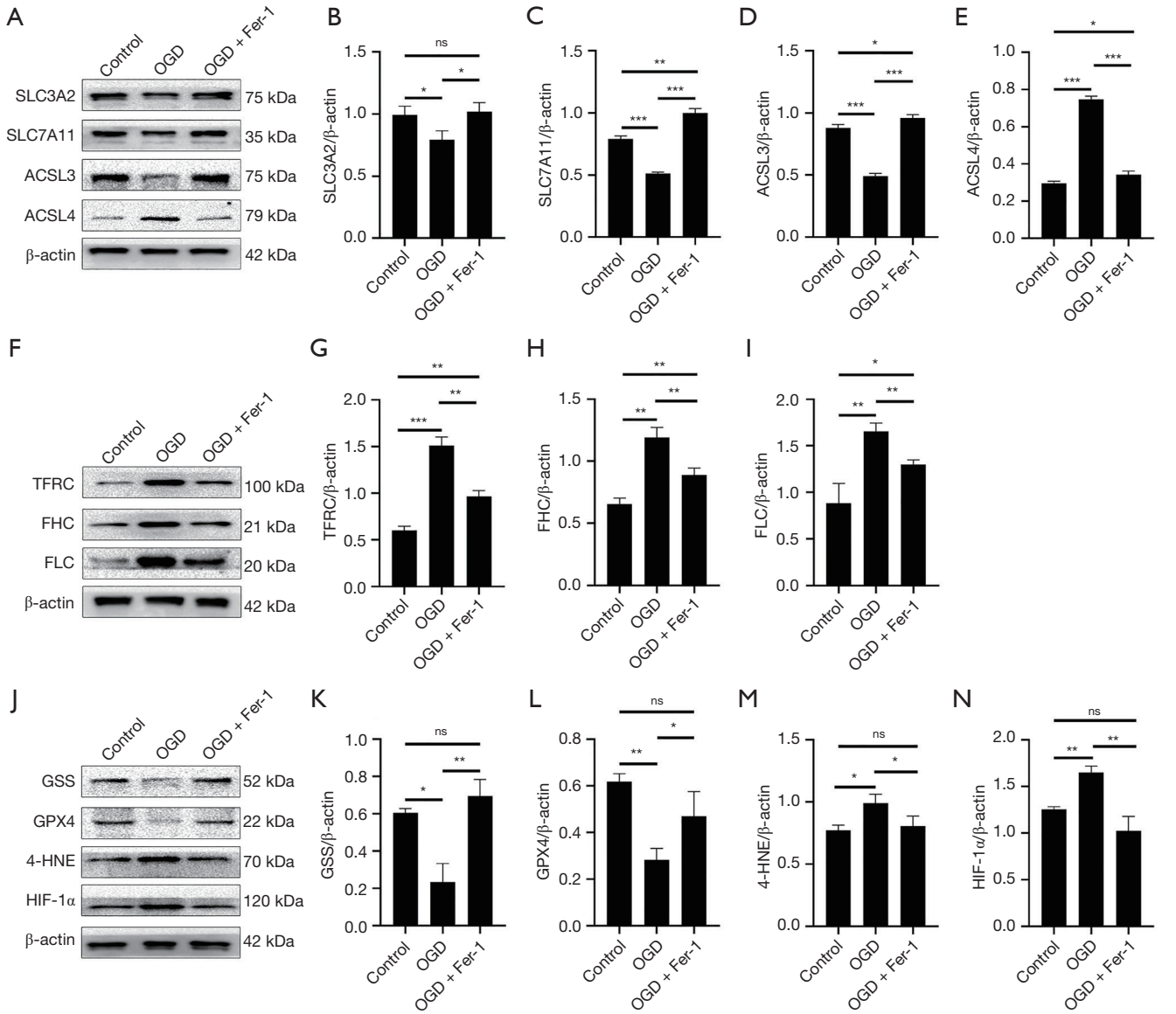

Figure 8 Fer-1 attenuates OGD-induced ferroptosis. (A-N) Representative western blot images and quantitation of SLC3A2, SLC7A11, ACSL3, ACSL4, TFRC, FHC, FLC, GSS, GPX4, 4-HNE, and HIF-1α 12 h after OGD modeling (normalized to β-actin). Mean ± standard deviation, n=3. *, P<0.05; **, P<0.01; ***, P<0.001, indicate significant differences; ns represents no significant difference. OGD, oxygen-glucose deprivation; Fer-1, ferrostatin-1; SLC3A2, solute carrier family 3, member 2; SLC7A11, solute carrier family 7, member 11; ACSL3, acyl-CoA synthetase long-chain family member 3; ACSL4, acyl-CoA synthetase long-chain family member 4; TFRC, transferrin receptor; FHC, ferritin heavy chain; FLC, ferritin light chain; GSS, glutathione synthetase; GPX4, glutathione peroxidase 4; 4-HNE, 4-hydroxynonenal; HIF-1α, hypoxia-inducible factor-1α.

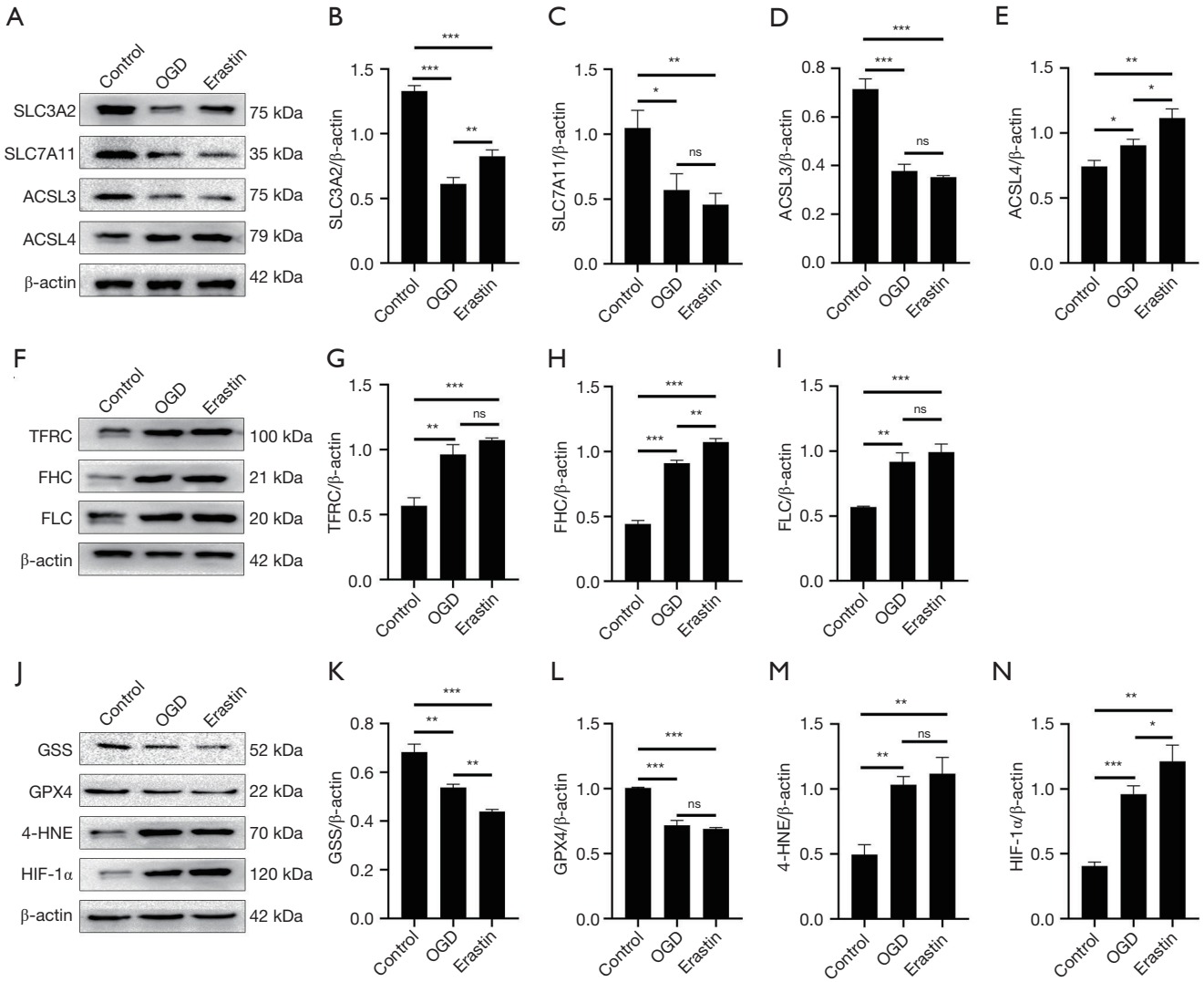

Figure 9 Both OGD and Erastin could induce ferroptosis. (A-N) Representative western blot images and quantitation of SLC3A2, SLC7A11, ACSL3, ACSL4, TFRC, FHC, FLC, GSS, GPX4, 4-HNE, and HIF-1α after 12 h of OGD and Erastin (normalized to β-actin). Mean ± standard deviation, n=3. *, P<0.05; **, P<0.01; ***, P<0.001, indicate significant differences; ns represents no significant difference. OGD, oxygen-glucose deprivation; SLC3A2, solute carrier family 3, member 2; SLC7A11, solute carrier family 7, member 11; ACSL3, acyl-CoA synthetase long-chain family member 3; ACSL4, acyl-CoA synthetase long-chain family member 4; TFRC, transferrin receptor; FHC, ferritin heavy chain; FLC, ferritin light chain; GSS, glutathione synthetase; GPX4, glutathione peroxidase 4; 4-HNE, 4-hydroxynonenal; HIF-1α, hypoxia-inducible factor-1α.

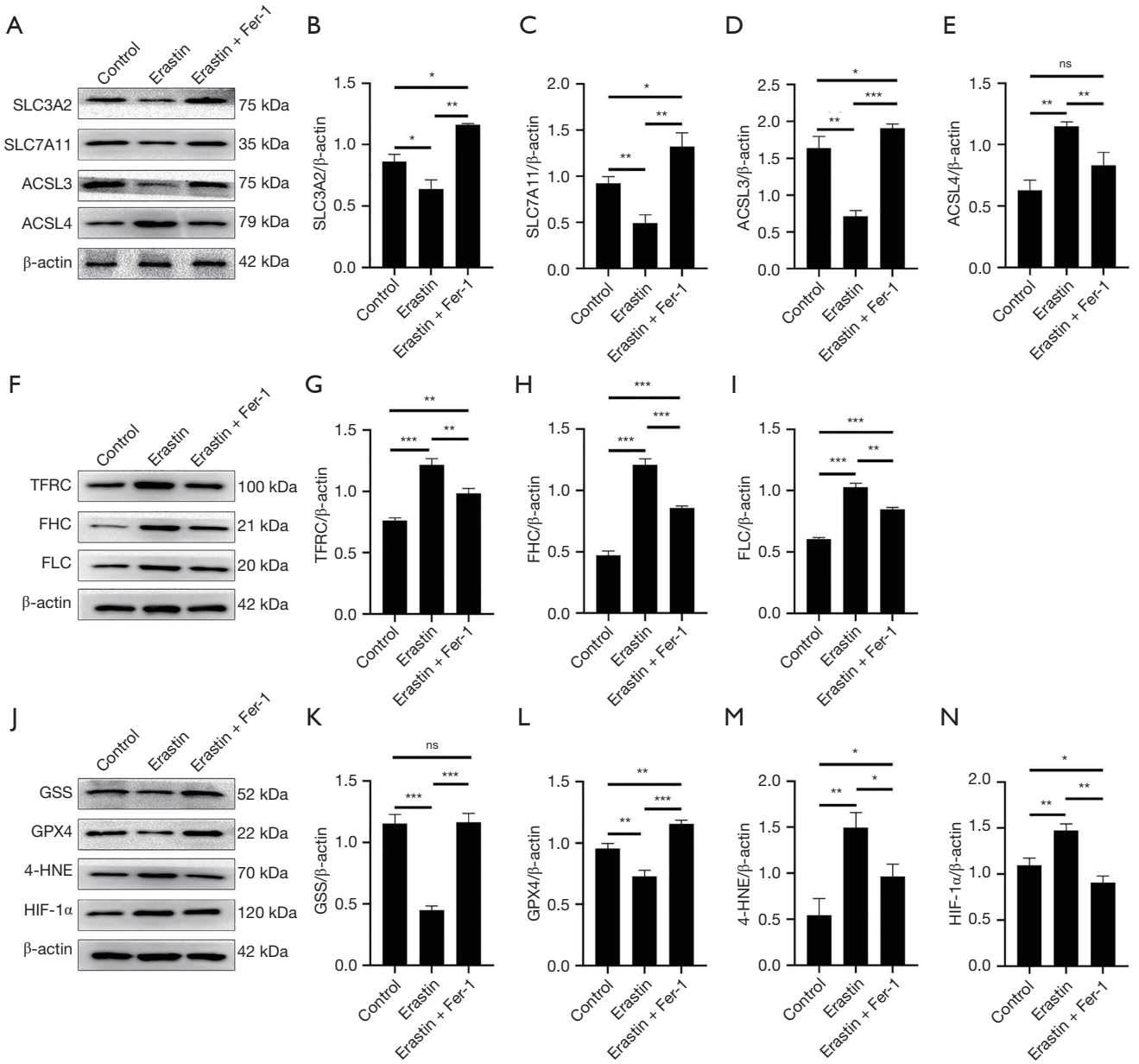

Figure 10 Fer-1 attenuates Erastin-induced ferroptosis. (A-N) Representative western blot images and quantitation of SLC3A2, SLC7A11, ACSL3, ACSL4, TFRC, FHC, FLC, GSS, GPX4, 4-HNE, and HIF-1α after 12 h Erastin treatment (normalized to β-actin). Mean ± standard deviation, n=3. *, P<0.05; **, P<0.01; ***, P<0.001, indicate significant differences; ns represents no significant difference. Fer-1, ferrostatin-1; SLC3A2, solute carrier family 3, member 2; SLC7A11, solute carrier family 7, member 11; ACSL3, acyl-CoA synthetase long-chain family member 3; ACSL4, acyl-CoA synthetase long-chain family member 4; TFRC, transferrin receptor; FHC, ferritin heavy chain; FLC, ferritin light chain; GSS, glutathione synthetase; GPX4, glutathione peroxidase 4; 4-HNE, 4-hydroxynonenal; HIF-1α, hypoxia-inducible factor-1α.

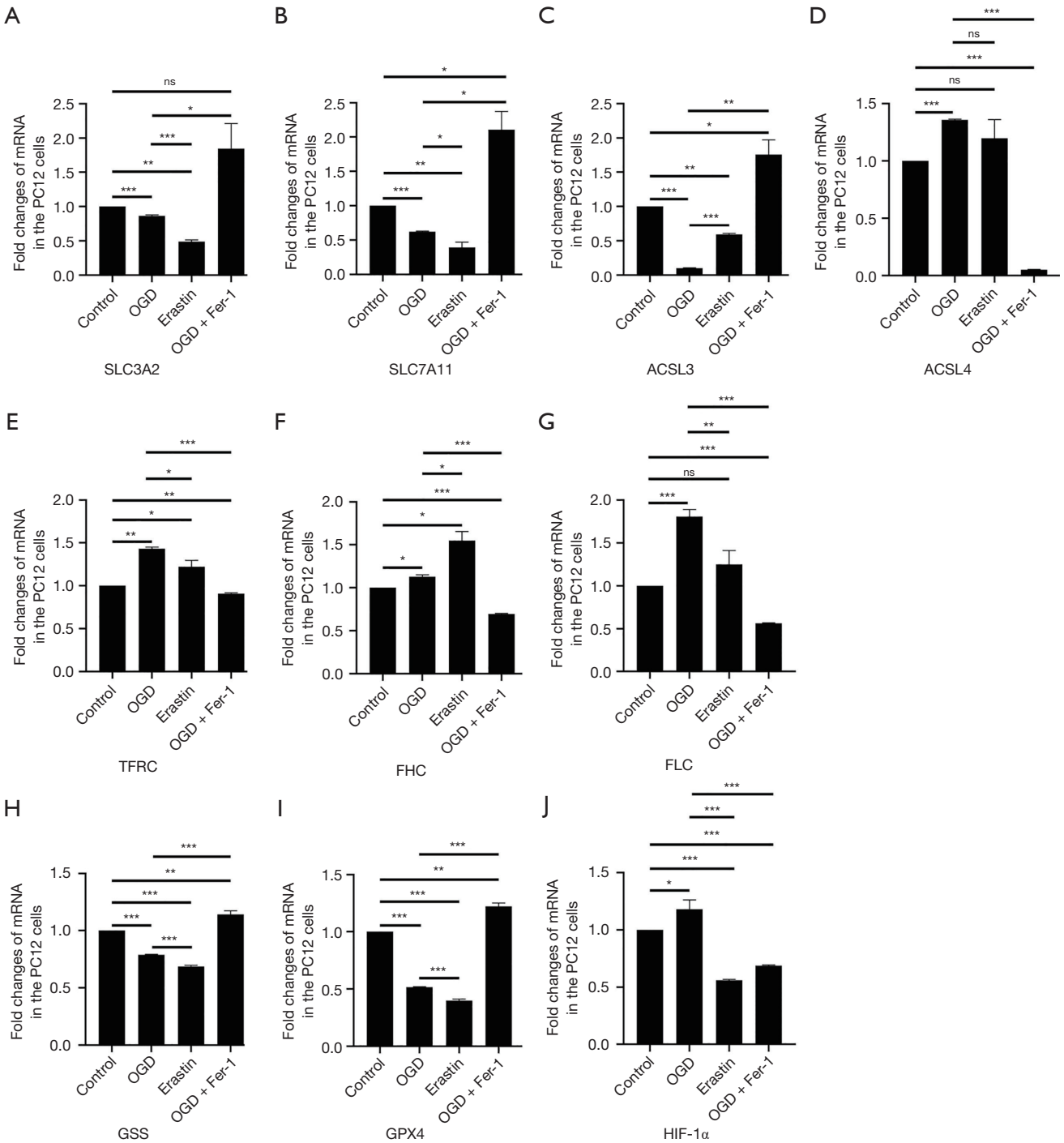

Figure 11 Change of mRNA expression levels of the ferroptosis-related gene in different groups *in vitro*. (A-J) The levels of SLC3A2, SLC7A11, ACSL3, ACSL4, TFRC, FHC, FLC, GSS, GPX4 and HIF-1α of mRNA expression in PC12 cells normalized to the expression of β-actin in each sample. Mean ± standard deviation, n=3. *, P<0.05; **, P<0.01; ***, P<0.001, indicate significant differences; ns represents no significant difference. mRNA, messenger RNA; OGD, oxygen-glucose deprivation; Fer-1, ferrostatin-1; SLC3A2, solute carrier family 3, member 2; SLC7A11, solute carrier family 7, member 11; ACSL3, acyl-CoA synthetase long-chain family member 3; ACSL4, acyl-CoA synthetase long-chain family member 4; TFRC, transferrin receptor; FHC, ferritin heavy chain; FLC, ferritin light chain; GSS, glutathione synthetase; GPX4, glutathione peroxidase 4; HIF-1α, hypoxia-inducible factor-1α.

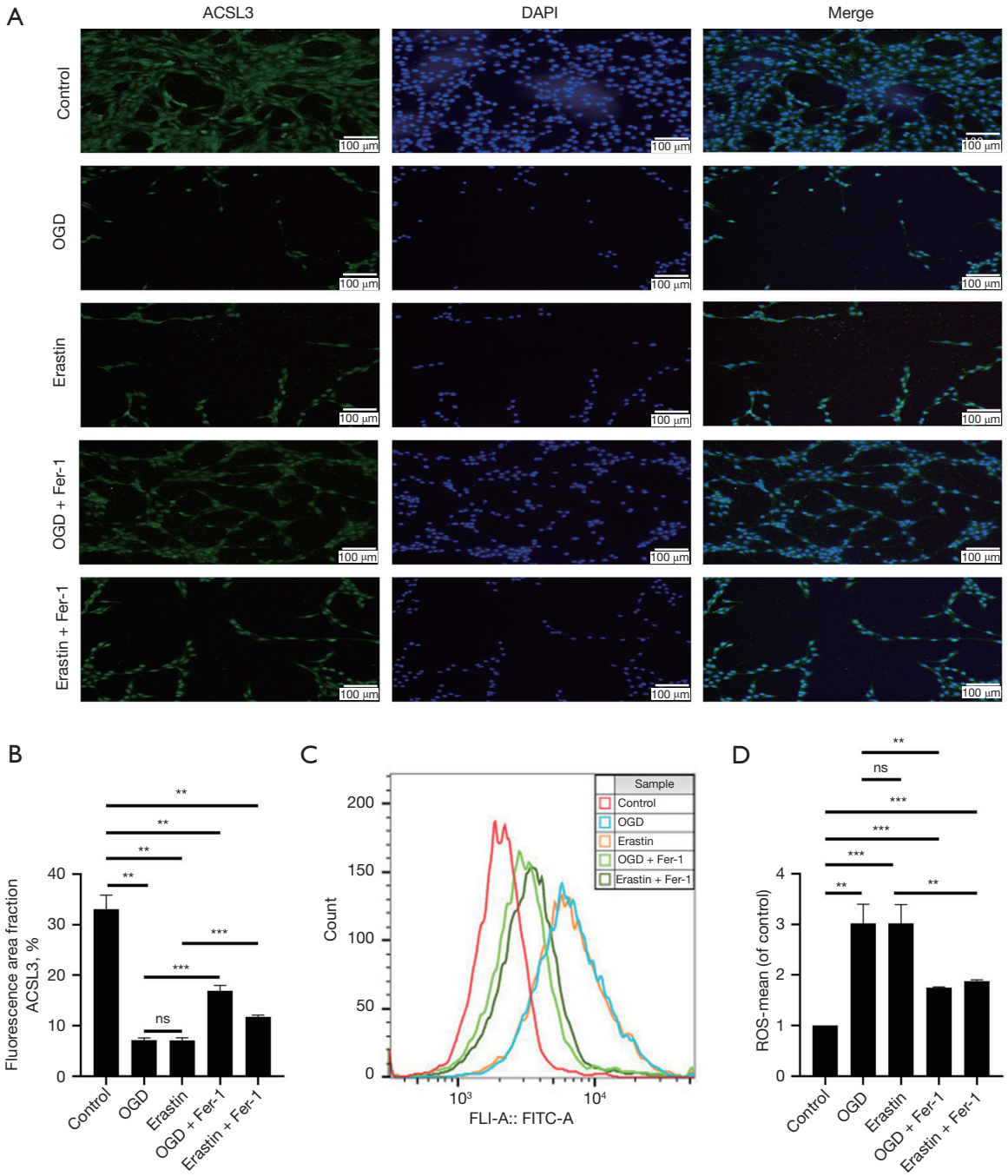

Figure 12 Fer-1 can alleviate the oxidative stress induced by the OGD model and Erastin. (A,B) The representative immunofluorescent staining images of ACSL3 (green) and DAPI (blue) 12 h after OGD/Erastin and the quantitative histogram of fluorescence staining. (C,D) Flow cytometry analysis and quantitative analysis of DCF-DA staining and the ROS in different groups (normalized to the Control group). Mean ± standard deviation, n=3. **, P<0.01; ***, P<0.001, indicate significant differences; ns represents no significant difference. OGD, oxygen-glucose deprivation; Fer-1, ferrostatin-1; ACSL3, acyl-CoA synthetase long-chain family member 3; DAPI, 4',6-diamidino-2-phenylindole; FL, fluorescence; FITC-A, fluorescein isothiocyanate; DCF-DA, 2',7'-dichlorofluorescein diacetate; ROS, reactive oxygen species.

TFRC and transferrin (TF) mainly participate in iron transport and promote susceptibility to ferroptosis (43,44). After HIBD/OGD modeling and Erastin intervention, the expression of TFRC at protein and mRNA level was significantly upregulated, and Fer-1 treatment abolished this effect (*Figures 4-11*).

Ferritin consists of two subunits, an H-chain (FHC) and an L-chain (FLC), and is the main reservoir of ferritin (45). Compared with the Sham group, the protein and mRNA expressions of FHC and FLC were significantly increased in the HIBD/OGD model and Erastin-treated groups. In contrast, Fer-1 reversed this trend (*Figures 4-11*).

Fer-1 alleviated oxidative stress injury

GSH is one of the most important antioxidants. GSH is primarily produced in two phases, with the final step being facilitated by the enzyme GSS (46). Genetic studies conducted on mice and cells have validated that GPX4 plays a pivotal role in regulating ferroptosis (47). Maintaining the proper function of GPX4, along with the synthesis of GSH and an adequate supply of cysteine, is crucial to the regulation of ferroptosis. Any inhibition or destabilization of GPX4 can initiate ferroptosis, leading to cellular damage (47). Our results showed that after hypoxia-ischemia injury *in vivo* and *in vitro* or application of ferroptosis inducer (Erastin), the protein and mRNA expressions of GSS and GPX4 were significantly upregulated, but decreased following Fer-1 intervention (*Figures 4-11*).

Polyunsaturated fatty acids (PUFAs) in the cell membrane accelerate lipid peroxidation and produce many toxic aldehydes [such as 4-hydroxy-2-nonenal (4-HNE)] in response to oxidative stress injury (46). Compared with the Sham group, the expression of 4-HNE protein was significantly increased after hypoxia-ischemia injury *in vitro* and *in vivo* and treatment with Erastin. However, the expression of 4-HNE was significantly downregulated by the ferroptosis inhibitor (Fer-1) (*Figures 4-6*,*8-10*).

HIF-1α is an oxygen-sensitive transcription factor that mediates the adaptive response of the body to hypoxia (47). In this study, the expression of HIF-1α protein was significantly increased following hypoxia-ischemia modeling *in vivo* and *in vitro* and treatment with ferroptosis inducer (Erastin). Ferroptosis inhibitor (Fer-1) reversed this trend (*Figures 4-10*). In the cell experiments, we found that after Erastin treatment, the expression of HIF-1α mRNA was not significantly increased, which was inconsistent with the protein expression. This might be due to the excessive mRNA consumption during translation (*Figure 11J*).

Fer-1 is an aromatic amine, which can specifically bind to lipid ROS and protect cells from lipid peroxidation damage (48). Studies have shown that ROS can accelerate the decomposition of iron storage protein ferritin and promote the release of iron, leading to the accumulation of redox active iron in cells. Fenton reaction-induced lipid peroxidation and GSH consumption can trigger ferroptosis (49). Here, flow cytometry analysis revealed that ROS production was significantly increased after modeling with OGD, and treatment with the ferroptosis inducer, and Fer-1 significantly reduced ROS production (*Figure 12C*,*12D*).

Fer-1 inhibited ferroptosis induced by OGD

Results of the TEM showed significant disruptions in the mitochondrial structure, characterized by swelling, matrix dissolution, and disappearance of cristae, following OGD modeling and treatment with a ferroptosis inducer (Erastin). The application of ferroptosis inhibitors (Fer-1) notably ameliorated mitochondrial swelling, matrix lysis, and cristae fractures (*Figure 13*). Based on the above *in vitro* and *in vivo* research results and the following discussion, we draw the potential mechanism diagram of Fer-1 in HIBD and OGD models, as shown in *Figure 14*.

Discussion

HIBD is a common, yet fatal disease of the nervous system, and it is one of the main causes of neonatal death. Survivors often develop severe sequelae (such as mental retardation and cerebral palsy) that may seriously affect their quality of life (50). Neonatal HIBD is primarily driven by neuroinflammation, which is initiated by ischemia and hypoxia. These conditions prompt rapid activation of immune cells in the brain, encompassing microglia, astrocytes, oligodendrocytes, as well as white blood cells and lymphocytes in the peripheral blood. The activated immune cells in both the brain and peripheral blood release a cascade of inflammatory factors, such as IL-1β, IL-6, and TNF-α, culminating in neuroinflammation following HIBD (51). HIBD can destroy the blood-brain barrier and release chemokines, and a large number of peripheral immune cells can enter the central nervous system to trigger an immune response (52). In addition, oxidative stress contributes to the pathophysiological mechanism of HIBD. There is compelling evidence that during hypoxia and

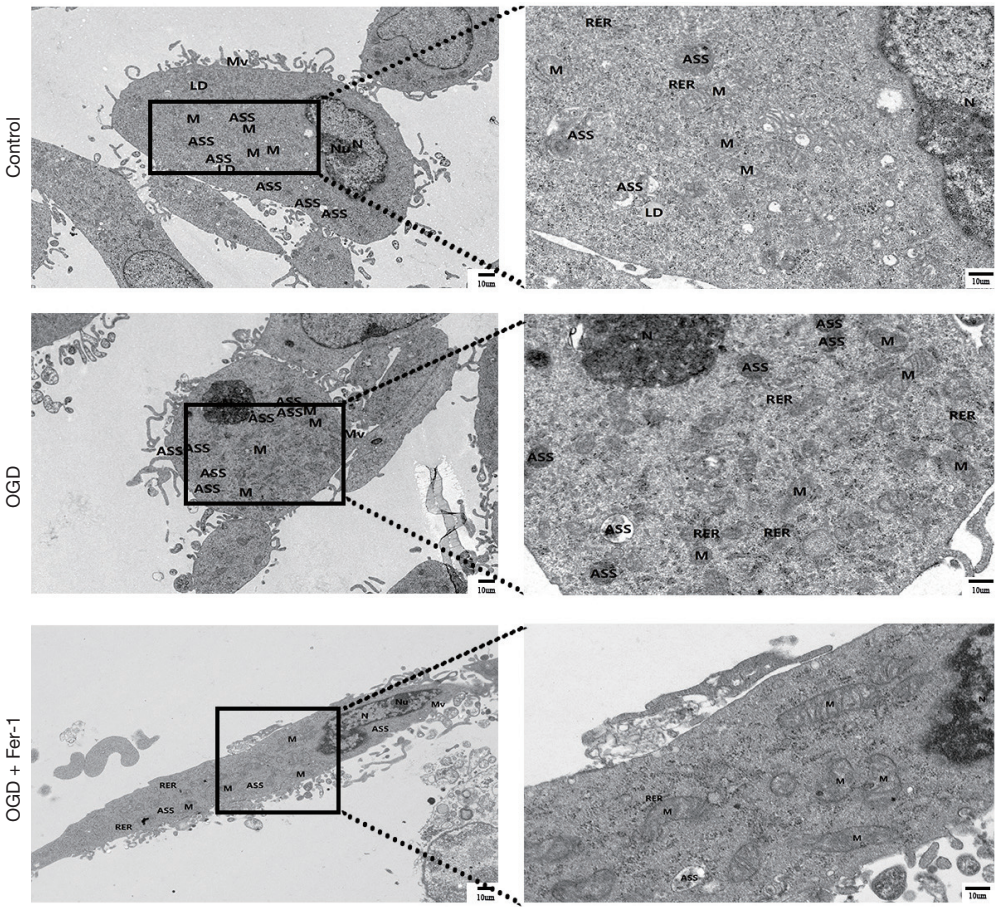

Figure 13 Representative TEM images of PC12 cells in different groups 12 h after OGD modeling. Different cellular structures are labeled. Scale bar 10 μm. Mv, microvillus; LD, lipid droplet; M, mitochondria; ASS, autolysosome; N, nucleus; Nu, nucleolus; RER, rough endoplasmic reticulum; OGD, oxygen-glucose deprivation; Fer-1, ferrostatin-1; TEM, transmission electron microscopy.

ischemia, NOX, NOS, and hypoxic mitochondrial electron transfer system are the main sources of ROS in the brain (53-55), and these oxygen free radicals can increase the expression of pro-inflammatory factors (56). Furthermore, oxidative stress disrupts both the structure and function of mitochondria, exacerbating damage to nerve tissues and cells (57). This study elucidates the involvement of ferroptosis and oxidative stress in the injury mechanism of HIBD. Notably, Fer-1 demonstrates the potential to ameliorate brain injury following hypoxia-ischemia modeling.

Fer-1 is a synthetic compound identified through high-throughput screening of small-molecule libraries. It can efficiently inhibit cell death. Although Fer-1 is a classical hydrogen peroxide radical scavenger, its mechanism does not appear to explain the observed inhibition of ferroptosis. Miotto *et al.* found that Fer-1 can eliminate lipid hydrogen peroxide in the presence of reduced iron and elicit the same anti-ferroptosis effect as GPX4 (58). However, the specific role and mechanism of Fer-1 in HIBD have not been clarified. In this study, we developed an *in vitro* and *in vivo* model for investigating the protective effects and potential mechanisms of Fer-1 on hypoxic-ischemic brain injury. At 72 h after HIBD, rats exhibited marked brain atrophy, liquefaction, and necrosis. The administration of Fer-1 facilitated the restoration of structural integrity and morphology, both in brain tissue and PC12 cell mitochondria, resulting in a reduction in the incidence of cellular degeneration and necrosis. These findings substantiate Fer-1's potential to effectively suppress ferroptosis, thereby enhancing recovery from HIBD.

System Xc^- is an important intracellular antioxidant

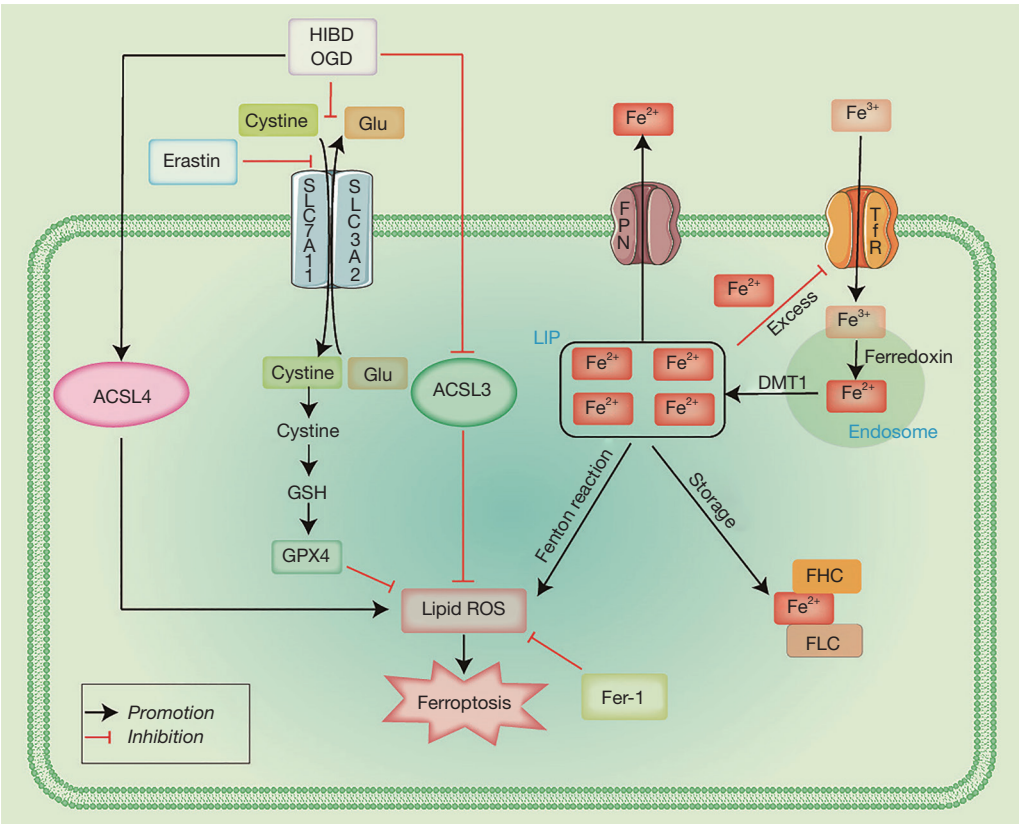

Figure 14 Mechanism diagram of Fer-1 and Erastin functions in HIBD/OGD models. HIBD, hypoxic-ischemic brain damage; OGD, oxygen-glucose deprivation; SLC7A11, solute carrier family 7, member 11; SLC3A2, solute carrier family 3, member 2; ACSL4, acyl-CoA synthetase long-chain family member 4; ACSL3, acyl-CoA synthetase long-chain family member 3; GSH, glutathione; GPX4, glutathione peroxidase 4; ROS, reactive oxygen species; Fer-1, ferrostatin-1; FPN, ferroportin; FHC, ferritin heavy chain; FLC, ferritin light chain; DMT1, divalent metal transporter 1; TfR, transferrin receptor.

system, also known as cystine/glutamic acid reverse transporter protein, which is mainly composed of heavy chain SLC3A2 and light chain SLC7A11. It is also the substrate for the synthesis of GSH (59). In mice, System Xc^- is mainly distributed in the spleen and thymus, but it is lowly expressed in the heart, kidney, liver, and lung. In human, System Xc^- is highly expressed in the brain and spinal cord, but is also detected in thymus, spleen, and lymph nodes (59). To date, the System Xc has been reported to play an important role in many diseases, including neurodegenerative diseases, cancer, stroke, and myocardial infarction (59). Through *in vitro* and *in vivo* experiments, we demonstrated that both the hypoxia-ischemia model and ferroptosis inducer Erastin inhibited the expression of SLC7A11 and SLC3A2, whereas Fer-1 treatment significantly increased the activity of System Xc^-. A study by Li *et al.* found that the expression levels of SLC3A2 and SLC7A11 were significantly decreased in the HIBD model, which was consistent with the experimental results in this study (57). Lin *et al.* also demonstrated that the expression of SLC3A2 was down-regulated after HIBD (11). However, Fitzgerald *et al.* found that hypoxia upregulated SLC3A2 expression (60). Based on this, we speculate that HIBD and Erastin can decrease the activity of System Xc^-, inhibit GSH synthesis, and increase lipid peroxidation products, leading to the occurrence of ferroptosis.

We further explored the mechanism by which Fer-1 inhibits ferroptosis. GPX4 can detoxify lipid peroxidation using GSH and suppress ferroptosis (61). Magtanong *et al.* found that ACSL3 was required by exogenous MUFAs to protect cells from ferroptosis, and the ACSL3-dependent MUFA metabolism is an important regulator of ferroptosis (39). It has been reported that ACSL4 activates PUFAs (62). Therefore, PUFAs cannot be integrated

into the membrane phospholipids after the deletion of ACSL4, and the PUFAs are oxidized after inactivation of GPX4 (39). In this study, we found through *in vitro* and *in vivo* experiments that Fer-1 increased the expression of GPX4 and ACSL3, and decreased the expression of ACSL4. These results suggested that Fer-1 confers a neuroprotective effect by inhibiting ferroptosis through the GPX4/ACSL3/ACSL4 axis.

Although iron is an essential trace element in the human body, excessive accumulation iron can lead to oxidative damage. Thus, iron homeostasis influences the activity and expression levels of the iron carrier, TF, and ferritin (63). TFRC is a plasma surface iron-loaded TF dimer glycoprotein receptor, and its extracellular region has a high affinity for di-iron TF (64). The ferritin composed of FHC and FLC is an intracellular ferritin. FHC can convert Fe^{2+} into Fe^{3+} and possesses iron oxygenase activity (64). Knockout of the FLC gene in mice resulted in brain and systemic iron metabolism disorders (65). Nevertheless, in cases of genetic iron element disorders, mutations in the human FLC gene may arise (66). In this study, Fer-1 demonstrated inhibitory effects on the expressions of TFRC, FHC, and FLC. Intriguingly, Lin *et al.* similarly observed notable increases in the expressions of FHC and FLC following HIBD modeling (11). These findings collectively indicate that Fer-1 plays a role in safeguarding against HIBD through the modulation of iron metabolism. Ferroptosis has three basis features: lipid peroxide clearance dysfunction, enrichment of redox-active iron, and oxidation of PUFA-containing phospholipids. One study has demonstrated that iron metabolism and lipid peroxidation are important regulatory mechanisms of ferroptosis (67). ROS regulates cell signal transduction and differentiation, as well as cell and gene damage processes, among others. It is also implicated in the pathophysiological processes of many diseases (66). Through protein-protein interaction analysis, Wu *et al.* found that GPX4 regulated the GSS/GSR complex and the downstream GGT family proteins (68). 4-HNE is a compound derived from PUFAs and can react with nucleic acids, phospholipids, and proteins. As a second messenger, 4-HNE participates in the process of inflammation by transmitting ROS signals (69). As the main regulator of oxygen homeostasis, HIF-α has become a hot topic in the current research (66). In this study, we found that after HIBD and Erastin treatment, the expression of GSS decreased, and that of ROS, 4-HNE, and HIF-α significantly increased. These results indicated that Fer-1 played a neuroprotective role by inhibiting oxidative stress after hypoxia-ischemia injury.

Reduced GSH is the most important antioxidant in the body. As a low molecular free radical scavenger, it can inhibit the formation of lipid peroxidation, to prevent oxygen free radicals-induced damage to tissues. It can also increase the activity of oxidase and inhibit the production of oxygen free radicals, thereby protect the brain. A combination of reduced GSH (300 mg) and ganglioside (20 mg) activated ATPase on brain cell membrane after brain tissue injury, leading to the alleviation of nerve cell edema (70). Melatonin, as an endogenous indoleamine, can directly scavenge free radicals through receptor-independent action and exert neuroprotective effect (71). Magnesium sulfate can bind to the magnesium site on the glutamic acid channel of N-methyl-d-aspartic acid (NMDA), which results in inhibition of the generation of free radicals, and stabilizes the cell membrane to prevent secondary inflammation associated with under oxidative stress (72). Edaravone is a free radical scavenger known to produce a free radical intermediate that interacts with peroxide, hydroxyl radical, lipid peroxide and DNA peroxide to form a stable oxidation product which confers a neuroprotective effect (73). Allopurinol is a xanthine oxidase inhibitor, which can directly scavenge free radicals to exert neuroprotection (74). In this study, we found that Fer-1 recovered the antioxidant levels and lipid peroxidation products after HIBD, indicating that Fer-1 improved HIBD by inhibiting ferroptosis *in vivo* and *in vitro*. Thus, Fer-1 is expected to be an important agent for clinic treatment of HIBD.

Although *in vivo* and *in vitro* experiments in this study demonstrated that Fer-1 improved HIBD by inhibiting ferroptosis via the GPX4/ACSL3/ACSL4 axis, there are some limitations that should be mentioned. First, PC12 cell lines were selected rather than primary cells for cellular experiments. Thus, *in vivo* pathogenesis should be explored to collaborate the results of *in vitro* experiments. Secondly, the tissues selected in this experiment were all obtained the cerebral cortex, and the specific brain tissue site of ferroptosis injury was not further clarified. Thirdly, the specific molecular mechanism of ferroptosis in HIBD was not elucidated in this study.

Conclusions

This study shows that hypoxia-ischemia injury and Erastin can induce significant changes in the expression of proteins associated with the GPX4/ACSL3/ACSL4 axis and increase

the products of oxidative stress, leading to enhanced ROS production and induction of ferroptosis. Fer-1 treatment can inhibit oxidative stress injury and suppress ferroptosis by activating the GPX4/ACSL3/ACSL4 axis. In summary, we infer that Fer-1 inhibits ferroptosis through the GPX4/ACSL3/ACSL4 axis, improves HIBD-or OGD-induced ferroptosis in neurons, and prevents HIBD.

Acknowledgments

Funding: This study was supported by the National Natural Science Foundation of China (No. 82271747), the National Natural Science Foundation of China (No. 82201902), and the Zhejiang Provincial Medicine and Health Plan Project (No. 2022KY448).

Footnote

Reporting Checklist: The authors have completed the ARRIVE reporting checklist. Available at https://tp.amegroups.com/article/view/10.21037/tp-23-189/rc

Data Sharing Statement: Available at https://tp.amegroups.com/article/view/10.21037/tp-23-189/dss

Peer Review File: Available at https://tp.amegroups.com/article/view/10.21037/tp-23-189/prf

Conflicts of Interest: All authors have completed the ICMJE uniform disclosure form (available at https://tp.amegroups.com/article/view/10.21037/tp-23-189/coif). The authors have no conflicts of interest to declare.

Ethical Statement: The authors are accountable for all aspects of the work in ensuring that questions related to the accuracy or integrity of any part of the work are appropriately investigated and resolved. All animal experiments were conducted under a project license (Ethics Batch No. wydw2022-0211) granted by the ethics committee of Wenzhou Medical University, in compliance with institutional guidelines for the care and use of animals.

References

1. Gu Y, He M, Zhou X, et al. Endogenous IL-6 of mesenchymal stem cell improves behavioral outcome of hypoxic-ischemic brain damage neonatal rats by supressing apoptosis in astrocyte. Sci Rep 2016;6:18587.
2. Yin X, Meng F, Wei W, et al. Role of mouse nerve growth factor in neural recovery following hypoxic-ischemic brain damage. Int J Clin Exp Med 2013;6:951-5.
3. Pappas A, Shankaran S, McDonald SA, et al. Cognitive outcomes after neonatal encephalopathy. Pediatrics 2015;135:e624-34.
4. Cai Y, Li X, Tan X, et al. Vitamin D suppresses ferroptosis and protects against neonatal hypoxic-ischemic encephalopathy by activating the Nrf2/HO-1 pathway. Transl Pediatr 2022;11:1633-44.
5. Li H, Li Q, Du X, et al. Lithium-mediated long-term neuroprotection in neonatal rat hypoxia-ischemia is associated with antiinflammatory effects and enhanced proliferation and survival of neural stem/progenitor cells. J Cereb Blood Flow Metab 2011;31:2106-15.
6. Hagberg H, Mallard C, Rousset CI, et al. Mitochondria: hub of injury responses in the developing brain. Lancet Neurol 2014;13:217-32.
7. Bi D, Qiao L, Bergelson I, et al. Staphylococcus epidermidis Bacteremia Induces Brain Injury in Neonatal Mice via Toll-like Receptor 2-Dependent and -Independent Pathways. J Infect Dis 2015;212:1480-90.
8. Albertsson AM, Zhang X, Vontell R, et al. γδ T Cells Contribute to Injury in the Developing Brain. Am J Pathol 2018;188:757-67.
9. Zhu K, Zhu X, Sun S, et al. Inhibition of TLR4 prevents hippocampal hypoxic-ischemic injury by regulating ferroptosis in neonatal rats. Exp Neurol 2021;345:113828.
10. Li C, Wu Z, Xue H, et al. Ferroptosis contributes to hypoxic-ischemic brain injury in neonatal rats: Role of the SIRT1/Nrf2/GPx4 signaling pathway. CNS Neurosci Ther 2022;28:2268-80.
11. Lin W, Zhang T, Zheng J, et al. Ferroptosis is Involved in Hypoxic-ischemic Brain Damage in Neonatal Rats. Neuroscience 2022;487:131-42.
12. Zhang M, Lin W, Tao X, et al. Ginsenoside Rb1 inhibits ferroptosis to ameliorate hypoxic-ischemic brain damage in neonatal rats. Int Immunopharmacol 2023;121:110503.

13. Dixon SJ, Lemberg KM, Lamprecht MR, et al. Ferroptosis: an iron-dependent form of nonapoptotic cell death. Cell 2012;149:1060-72.
14. Tang D, Chen X, Kang R, et al. Ferroptosis: molecular mechanisms and health implications. Cell Res 2021;31:107-25.
15. Li J, Cao F, Yin HL, et al. Ferroptosis: past, present and future. Cell Death Dis 2020;11:88.
16. Ke F, Wang H, Geng J, et al. MiR-155 promotes inflammation and apoptosis via targeting SIRT1 in hypoxic-ischemic brain damage. Exp Neurol 2023;362:114317.
17. Yu L, Liu S, Zhou R, et al. Atorvastatin inhibits neuronal apoptosis via activating cAMP/PKA/p-CREB/BDNF pathway in hypoxic-ischemic neonatal rats. FASEB J 2022;36:e22263.
18. Wu G, Chen Z, Wang P, et al. Hydrogen inhalation protects hypoxic-ischemic brain damage by attenuating inflammation and apoptosis in neonatal rats. Exp Biol Med (Maywood) 2019;244:1017-27.
19. Dai Y, Hu L. HSPB1 overexpression improves hypoxic-ischemic brain damage by attenuating ferroptosis in rats through promoting G6PD expression. J Neurophysiol 2022;128:1507-17.
20. Zhu K, Zhu X, Liu S, et al. Glycyrrhizin Attenuates Hypoxic-Ischemic Brain Damage by Inhibiting Ferroptosis and Neuroinflammation in Neonatal Rats via the HMGB1/GPX4 Pathway. Oxid Med Cell Longev 2022;2022:8438528.
21. Sun M, An Z, Wei H, et al. Xenon attenuates hypoxic-ischemic brain damage by inhibiting autophagy in neonatal rats. Neuroreport 2023;34:273-9.
22. Fu CH, Lai FF, Chen S, et al. Silencing of long non-coding RNA CRNDE promotes autophagy and alleviates neonatal hypoxic-ischemic brain damage in rats. Mol Cell Biochem 2020;472:1-8.
23. Wei W, Lu M, Lan X, et al. Neuroprotective effect of Verbascoside on hypoxic-ischemic brain damage in neonatal rat. Neurosci Lett 2019;711:134415.
24. Zhu JJ, Yu BY, Huang XK, et al. Neferine Protects against Hypoxic-Ischemic Brain Damage in Neonatal Rats by Suppressing NLRP3-Mediated Inflammasome Activation. Oxid Med Cell Longev 2021;2021:6654954.
25. Zhong Y, Wang S, Yin Y, et al. Dexmedetomidine suppresses hippocampal astrocyte pyroptosis in cerebral hypoxic-ischemic neonatal rats by upregulating microRNA-148a-3p to inactivate the STAT/JMJD3 axis. Int Immunopharmacol 2023;121:110440.
26. Vannucci RC, Connor JR, Mauger DT, et al. Rat model of perinatal hypoxic-ischemic brain damage. J Neurosci Res 1999;55:158-63.
27. Liu P, Feng Y, Li H, et al. Ferrostatin-1 alleviates lipopolysaccharide-induced acute lung injury via inhibiting ferroptosis. Cell Mol Biol Lett 2020;25:10.
28. Xiao Z, Kong B, Fang J, et al. Ferrostatin-1 alleviates lipopolysaccharide-induced cardiac dysfunction. Bioengineered 2021;12:9367-76.
29. Wang H, Huo X, Han C, et al. Ferroptosis is involved in the development of neuropathic pain and allodynia. Mol Cell Biochem 2021;476:3149-61.
30. Ding Z, Liang X, Wang J, et al. Inhibition of spinal ferroptosis-like cell death alleviates hyperalgesia and spontaneous pain in a mouse model of bone cancer pain. Redox Biol 2023;62:102700.
31. Tuo QZ, Liu Y, Xiang Z, et al. Thrombin induces ACSL4-dependent ferroptosis during cerebral ischemia/reperfusion. Signal Transduct Target Ther 2022;7:59.
32. Ye L, Wang X, Cai C, et al. FGF21 promotes functional recovery after hypoxic-ischemic brain injury in neonatal rats by activating the PI3K/Akt signaling pathway via FGFR1/β-klotho. Exp Neurol 2019;317:34-50.
33. Eng LF. Glial fibrillary acidic protein (GFAP): the major protein of glial intermediate filaments in differentiated astrocytes. J Neuroimmunol 1985;8:203-14.
34. Douglas-Escobar MV, Heaton SC, Bennett J, et al. UCH-L1 and GFAP Serum Levels in Neonates with Hypoxic-Ischemic Encephalopathy: A Single Center Pilot Study. Front Neurol 2014;5:273.
35. Bridges RJ, Natale NR, Patel SA. System xc cystine/glutamate antiporter: an update on molecular pharmacology and roles within the CNS. Br J Pharmacol 2012;165:20-34.
36. Lewerenz J, Hewett SJ, Huang Y, et al. The cystine/glutamate antiporter system x(c)(-) in health and disease: from molecular mechanisms to novel therapeutic opportunities. Antioxid Redox Signal 2013;18:522-55.
37. Yang Y, Zhu T, Wang X, et al. ACSL3 and ACSL4, Distinct Roles in Ferroptosis and Cancers. Cancers (Basel) 2022;14:5896.
38. Klasson TD, LaGory EL, Zhao H, et al. ACSL3 regulates lipid droplet biogenesis and ferroptosis sensitivity in clear cell renal cell carcinoma. Cancer Metab 2022;10:14.
39. Magtanong L, Ko PJ, To M, et al. Exogenous Monounsaturated Fatty Acids Promote a Ferroptosis-Resistant Cell State. Cell Chem Biol 2019;26:420-432.e9.
40. Yuan H, Li X, Zhang X, et al. Identification of ACSL4

as a biomarker and contributor of ferroptosis. Biochem Biophys Res Commun 2016;478:1338-43.
41. Chen YC, Oses-Prieto JA, Pope LE, et al. Reactivity-Based Probe of the Iron(II)-Dependent Interactome Identifies New Cellular Modulators of Ferroptosis. J Am Chem Soc 2020;142:19085-93.
42. Xu X, Chen Y, Zhang Y, et al. Highly stable and biocompatible hyaluronic acid-rehabilitated nanoscale MOF-Fe2+ induced ferroptosis in breast cancer cells. J Mater Chem B 2020. [Epub ahead of print]. doi: 10.1039/d0tb01616k.
43. Hong X, Roh W, Sullivan RJ, et al. The Lipogenic Regulator SREBP2 Induces Transferrin in Circulating Melanoma Cells and Suppresses Ferroptosis. Cancer Discov 2021;11:678-95.
44. Tang LJ, Zhou YJ, Xiong XM, et al. Ubiquitin-specific protease 7 promotes ferroptosis via activation of the p53/TfR1 pathway in the rat hearts after ischemia/reperfusion. Free Radic Biol Med 2021;162:339-52.
45. Cozzi A, Corsi B, Levi S, et al. Overexpression of wild type and mutated human ferritin H-chain in HeLa cells: in vivo role of ferritin ferroxidase activity. J Biol Chem 2000;275:25122-9.
46. Li Y, Zhao T, Li J, et al. Oxidative Stress and 4-hydroxy-2-nonenal (4-HNE): Implications in the Pathogenesis and Treatment of Aging-related Diseases. J Immunol Res 2022;2022:2233906.
47. Zheng J, Chen P, Zhong J, et al. HIF-1α in myocardial ischemia-reperfusion injury (Review). Mol Med Rep 2021;23:352.
48. Li D, Song C, Zhang J, et al. ROS and iron homeostasis dependent ferroptosis play a vital role in 5-Fluorouracil induced cardiotoxicity in vitro and in vivo. Toxicology 2022;468:153113.
49. Yi J, Wu S, Tan S, et al. Berberine alleviates liver fibrosis through inducing ferrous redox to activate ROS-mediated hepatic stellate cells ferroptosis. Cell Death Discov 2021;7:374.
50. Yang L, Zhao H, Cui H. Treatment and new progress of neonatal hypoxic-ischemic brain damage. Histol Histopathol 2020;35:929-36.
51. Wang Y, Cao M, Liu A, et al. Changes of inflammatory cytokines and neurotrophins emphasized their roles in hypoxic-ischemic brain damage. Int J Neurosci 2013;123:191-5.
52. Liu F, McCullough LD. Inflammatory responses in hypoxic ischemic encephalopathy. Acta Pharmacol Sin 2013;34:1121-30.
53. Lu Q, Wainwright MS, Harris VA, et al. Increased NADPH oxidase-derived superoxide is involved in the neuronal cell death induced by hypoxia-ischemia in neonatal hippocampal slice cultures. Free Radic Biol Med 2012;53:1139-51.
54. Liu H, Li J, Zhao F, et al. Nitric oxide synthase in hypoxic or ischemic brain injury. Rev Neurosci 2015;26:105-17.
55. Wang Z, Feng C, Zhao H, et al. Autoregulation of inducible nitric oxide synthase expression by RNA interference provides neuroprotection in neonatal rats. Theranostics 2015;5:504-14.
56. Jin R, Yang G, Li G. Inflammatory mechanisms in ischemic stroke: role of inflammatory cells. J Leukoc Biol 2010;87:779-89.
57. Li LY, Wang Q, Deng L, et al. Chlorogenic acid alleviates hypoxic-ischemic brain injury in neonatal mice. Neural Regen Res 2023;18:568-76.
58. Miotto G, Rossetto M, Di Paolo ML, et al. Insight into the mechanism of ferroptosis inhibition by ferrostatin-1. Redox Biol 2020;28:101328.
59. Tu H, Tang LJ, Luo XJ, et al. Insights into the novel function of system Xc- in regulated cell death. Eur Rev Med Pharmacol Sci 2021;25:1650-62.
60. Fitzgerald E, Roberts J, Tennant DA, et al. Metabolic adaptations to hypoxia in the neonatal mouse forebrain can occur independently of the transporters SLC7A5 and SLC3A2. Sci Rep 2021;11:9092.
61. Zhang Y, Swanda RV, Nie L, et al. mTORC1 couples cyst(e)ine availability with GPX4 protein synthesis and ferroptosis regulation. Nat Commun 2021;12:1589.
62. Kang MJ, Fujino T, Sasano H, et al. A novel arachidonate-preferring acyl-CoA synthetase is present in steroidogenic cells of the rat adrenal, ovary, and testis. Proc Natl Acad Sci U S A 1997;94:2880-4.
63. Gao G, Li J, Zhang Y, et al. Cellular Iron Metabolism and Regulation. Adv Exp Med Biol 2019;1173:21-32.
64. Chen X, Yu C, Kang R, et al. Iron Metabolism in Ferroptosis. Front Cell Dev Biol 2020;8:590226.
65. Li W, Garringer HJ, Goodwin CB, et al. Systemic and cerebral iron homeostasis in ferritin knock-out mice. PLoS One 2015;10:e0117435.
66. Iacobini C, Vitale M, Haxhi J, et al. Mutual Regulation between Redox and Hypoxia-Inducible Factors in Cardiovascular and Renal Complications of Diabetes. Antioxidants (Basel) 2022;11:2183.
67. Yu Y, Yan Y, Niu F, et al. Ferroptosis: a cell death connecting oxidative stress, inflammation and cardiovascular diseases. Cell Death Discov 2021;7:193.

68. Wu W, Geng Z, Bai H, et al. Ammonium Ferric Citrate induced Ferroptosis in Non-Small-Cell Lung Carcinoma through the inhibition of GPX4-GSS/GSR-GGT axis activity. Int J Med Sci 2021;18:1899-909.
69. Reyes-Jiménez E, Ramírez-Hernández AA, Santos-Álvarez JC, et al. Involvement of 4-hydroxy-2-nonenal in the pathogenesis of pulmonary fibrosis. Mol Cell Biochem 2021;476:4405-19.
70. Min YJ, Ling EA, Li F. Immunomodulatory Mechanism and Potential Therapies for Perinatal Hypoxic-Ischemic Brain Damage. Front Pharmacol 2020;11:580428.
71. Alonso-Alconada D, Alvarez A, Arteaga O, et al. Neuroprotective effect of melatonin: a novel therapy against perinatal hypoxia-ischemia. Int J Mol Sci 2013;14:9379-95.
72. Cetinkaya M, Alkan T, Ozyener F, et al. Possible neuroprotective effects of magnesium sulfate and melatonin as both pre- and post-treatment in a neonatal hypoxic-ischemic rat model. Neonatology 2011;99:302-10.
73. Takizawa Y, Miyazawa T, Nonoyama S, et al. Edaravone inhibits DNA peroxidation and neuronal cell death in neonatal hypoxic-ischemic encephalopathy model rat. Pediatr Res 2009;65:636-41.
74. Chaudhari T, McGuire W. Allopurinol for preventing mortality and morbidity in newborn infants with suspected hypoxic-ischaemic encephalopathy. Cochrane Database Syst Rev 2008;(2):CD006817.

Cite this article as: Zhang M, Liu Z, Zhou W, Shen M, Mao N, Xu H, Wang Y, Xu Z, Li M, Jiang H, Chen Y, Zhu J, Lin W, Yuan J, Lin Z. Ferrostatin-1 attenuates hypoxic-ischemic brain damage in neonatal rats by inhibiting ferroptosis. Transl Pediatr 2023;12(11):1944-1970. doi: 10.21037/tp-23-189